


# Satellite glial cells in sensory ganglia express functional transient receptor potential ankyrin 1 that is sensitized in neuropathic and inflammatory pain

Seung Min Shin<sup>1,2</sup>, Brandon Itson-Zoske<sup>1</sup>, Yongsong Cai<sup>1,3</sup>,  
Chensheng Qiu<sup>1,4</sup>, Bin Pan<sup>1</sup>, Cheryl L Stucky<sup>5</sup>, Quinn H Hogan<sup>1,2</sup>,  
and Hongwei Yu<sup>1,2</sup> 

Molecular Pain  
Volume 16: 1–19  
© The Author(s) 2020  
Article reuse guidelines:  
sagepub.com/journals-permissions  
DOI: 10.1177/1744806920925425  
journals.sagepub.com/home/mpx  


## Abstract

Transient receptor potential ankyrin 1 (TRPA1) is well documented as an important molecule in pain hypersensitivity following inflammation and nerve injury and in many other cellular biological processes. Here, we show that TRPA1 is expressed not only by sensory neurons of the dorsal root ganglia (DRG) but also in their adjacent satellite glial cells (SGCs), as well as nonmyelinating Schwann cells. TRPA1 immunoreactivity is also detected in various cutaneous structures of sensory neuronal terminals, including small and large caliber cutaneous sensory fibers and endings. The SGC-expressed TRPA1 is functional. Like DRG neurons, dissociated SGCs exhibit a robust response to the TRPA1-selective agonist allyl isothiocyanate (AITC) by an increase of intracellular  $\text{Ca}^{2+}$  concentration ( $[\text{Ca}^{2+}]_i$ ). These responses are abolished by the TRPA1 antagonist HC030031 and are absent in SGCs and neurons from global TRPA1 null mice. SGCs and neurons harvested from DRG proximal to painful tissue inflammation induced by plantar injection of complete Freund's adjuvant show greater AITC-evoked elevation of  $[\text{Ca}^{2+}]_i$  and slower recovery compared to sham controls. Similar TRPA1 sensitization occurs in both SGCs and neurons during neuropathic pain induced by spared nerve injury. Together, these results show that functional TRPA1 is expressed by sensory ganglia SGCs, and TRPA1 function in SGCs is enhanced after both peripheral inflammation and nerve injury, and suggest that TRPA1 in SGCs may contribute to inflammatory and neuropathic pain.

## Keywords

Transient receptor potential ankyrin 1, dorsal root ganglia, satellite glial cells, primary sensory neurons, neuropathic pain, inflammatory pain

Date Received: 23 January 2020; Revised 31 March 2020; accepted: 2 April 2020

## Introduction

Chronic pain is a frequent consequence of peripheral nerve injury and inflammation. Dorsal root ganglia (DRG) are a site in the peripheral somatosensory pathway that is critically involved in the development and maintenance of chronic pain.<sup>1–3</sup> A unique feature of the DRG is that each sensory neuronal soma with its initial axon segment is ensheathed by several satellite glial cells (SGCs) that are interconnected each other via gap junctions, together forming a discrete anatomical and functional sensory unit.<sup>4–6</sup> This structure permits bidirectional communication and functional interactions between sensory neurons and SGCs, including activation

<sup>1</sup>Department of Anesthesiology, Medical College of Wisconsin, Milwaukee, WI, USA

<sup>2</sup>Clement J. Zablocki VA Medical Center, Milwaukee, WI, USA

<sup>3</sup>Xi'an Jiaotong University Health Science Center, Xi'an, P.R. China

<sup>4</sup>Department of Orthopedic Surgery, Affiliated Hospital of Qingdao University, Qingdao, P.R. China

<sup>5</sup>Department of Cell Biology, Neurobiology and Anatomy, Medical College of Wisconsin, Milwaukee, WI, USA

### Corresponding Authors:

Hongwei Yu, Department of Anesthesiology, Medical College of Wisconsin, Milwaukee, WI 53226, USA.

Email: hyu@mcw.edu

Quinn H Hogan, Department of Anesthesiology, Medical College of Wisconsin, Milwaukee, WI 53226, USA.

Email: qhogan@mcw.edu



of neighboring neurons and SGCs.<sup>7,8</sup> There is now growing evidence that normal neuronal activity in DRG depends on neuron–glia interactions and that abnormal SGC function may contribute to painful conditions.<sup>9–13</sup> Thus, there is a need to more fully understand the nature of SGC interactions with primary sensory neurons and their role in chronic pain.

SGCs share biological properties with astrocytes of central nervous system (CNS),<sup>14</sup> such as their common functions of regulating ion concentrations in the extracellular space, recycling of neurotransmitters, and proliferation/activation in response to injury. Astrocyte-expressed proteins and transporters for various neuroactive molecules (cytokines, ATP, bradykinins, etc.) have also been identified in SGCs.<sup>5,15</sup> Additionally, SGCs express various ion channels that were historically thought to be exclusively expressed in neurons, including channel protein belonging to the transient receptor potential (TRP) family, such as TRPV4.<sup>16</sup> With the development of potent and selective pharmacological reagents, new antibodies, and advanced molecular genetic techniques, new roles for various TRP channels have been revealed in diverse nonneuronal cells. For example, transient receptor potential ankyrin 1 (TRPA1) has been found expressed in CNS astrocytes functioning in regulating astrocyte calcium homeostasis.<sup>17,18</sup> TRPA1 has also been demonstrated to have wide expression in many other nonneuronal cells, such as keratinocytes, mast cells, dendritic cells, lung cells, and endothelial cells, where its multiple functions occur through regulation of nonneuronal cell activities.<sup>19,20</sup> Recent reports describe expression and function of TRPA1 in CNS oligodendrocytes<sup>21</sup> and peripheral nerve Schwann cells (SCs).<sup>22,23</sup> Human SCs also express TRPA1 and recapitulate the functions of mouse SCs.<sup>22</sup>

SGCs and SCs are both derived from neural crest stem cells during embryonic development and share similar gene expression pattern and cellular morphology.<sup>6,24</sup> The former ensheath the primary sensory neurons, and the latter are divided into two types, either myelinating SCs that enwrap large-diameter axons or nonmyelinating SCs that surround the nonmyelinated C fiber nociceptors. SGCs may represent a population of developmentally arrested SCs.<sup>24</sup> It is now recognized that TRPA1 is expressed by peripheral nerve SCs where it contributes to peripheral nerve injury-induced chronic pain states. However, significantly less is known whether TRPA1 is also expressed and functions in SGCs.

In the present study, we use a well-validated TRPA1 extracellular loop-epitope antibody and Fura-2 ratio-metric microfluorimetry to study TRPA1 expression and function, with a particular focus on the DRG SGC population and comparison to primary sensory neuronal TRPA1 expression as well. Our goals are to

first determine if TRPA1 is expressed in SGCs and, if so, to characterize its function in regulating calcium homeostasis in these cells, and finally to identify if SGC-TRPA1 is altered in inflammatory and neuropathic pain conditions. Our positive findings in these experiments support that SGC-TRPA1 may play a role in the pathophysiology of chronic pain, and targeting SGC-TRPA1 could be a potential strategy for treatment of chronic pain.

## Materials and methods

### Animals

Adult male Sprague Dawley rats (six to eight weeks old, Charles River Laboratories, Wilmington, MA, USA) and male mice in C57BL/6 background with TRPA1 null and their wild-type littermates (eight weeks old)<sup>25,26</sup> were used. All animal experiments were performed with the approval of the Zablocki VA Medical Center Animal Studies Subcommittee and Medical College of Wisconsin Institutional Animal Care and Use Committee in accordance with the National Institutes of Health Guidelines for the Care and Use of Laboratory Animals. Animals were housed individually in a room maintained at constant temperature ( $22 \pm 0.5^\circ\text{C}$ ) and relative humidity ( $60 \pm 15\%$ ) with an alternating 12 hr light–dark cycle. Animals were given access to water and food *ad libitum* throughout the experiment, and all efforts were made to minimize suffering and the numbers of animal used. For tissue harvest euthanasia, animals were deeply anesthetized by isoflurane followed by decapitation with a well-maintained guillotine. The numbers of rats used are detailed in the relevant sections of the experiments.

### Pain models

Inflammatory pain was induced by subcutaneous intraplantar injection of a single dose of complete Freund's adjuvant (CFA), performed as described previously.<sup>27</sup> Briefly, on day 0, after baseline behavior testing (von Frey, Pin, and Hargreaves heat), rats were anesthetized briefly with isoflurane (4% induction and 2% maintenance), their right foot was swabbed with ethanol, followed by injection of 100  $\mu\text{l}$  of CFA (Sigma-Aldrich, St. Louis, MO, USA) at a concentration of 1.0 mg/ml or saline subcutaneously in the plantar surface of the right hindpaw.<sup>28</sup> Behavior was evaluated thereafter every 2 days until 10 days post CFA.

Neuropathic pain was induced using the spared nerve injury (SNI) model, performed as described previously.<sup>29–31</sup> Briefly, after baseline behavior testing (von Frey, Pin, and Heat), the surgical field (right leg) of the isoflurane-anesthetized animal was shaved

and disinfected. The skin was incised at the lateral mid-thigh and the underlying muscles separated to expose the right sciatic nerve. The tibial and common peroneal nerves were then individually ligated with 6–0 sutures and transected distally to the ligature, and 2 to 3 mm of each nerve was removed from the distal segment of these nerves. Contact with the preserved sural nerve was avoided. Muscle and skin were then closed using 4.0 monofilament nylon sutures and wound clips. The rats were then monitored in their cages until fully emerged from anesthesia. Behavior was evaluated thereafter on a weekly basis until four weeks post SNI. Sham-operated rats were subjected to the same procedures but without nerve ligation and transection. Animals without surgery or manipulation are designated naïve rats.

### *Sensory behavioral testing*

Animals were habituated in individual test compartments for at least 1 hr before each testing. Behavioral tests for punctate mechanical perception (von Frey test), punctate mechanical nociception (Pin test), and heat nociception (Hargreaves test) were performed as previously described.<sup>32</sup> Specifically, the von Frey test was performed using calibrated monofilaments (Patterson Medical, Bolingbrook, IL, USA) beginning with the 2.8 g filament, which were applied with just enough force to bend the fiber and held for 1 s. If a response was observed, the next smaller filament was applied, and if no response was observed, the next larger was applied, until a reversal occurred, defined as a withdrawal after a previous lack of withdrawal, or vice versa. Following a reversal event, four more stimulations were performed following the same pattern. The forces of the filaments before and after the first reversal, and the four filaments applied thereafter, were used to calculate the 50% withdrawal threshold.<sup>33</sup> Rats not responding to any filament were assigned a score of 25 g. The Pin test was performed using the point of a 22 g spinal anesthesia needle that was gently applied to the center of plantar surface of the hindpaw without penetrating the skin. Five applications were separated by at least 10 s, which was repeated after 2 min, making a total of 10 touches. For each application, the induced behavior was either a very brisk, simple withdrawal with immediate return of the foot to the cage floor or a sustained elevation with grooming that included licking and chewing, and possibly shaking, which lasted at least 1 s. This behavior, termed a hyperalgesic response, is specifically associated with place avoidance,<sup>34</sup> indicating that it is aversive. This test was quantified by tabulating hyperalgesic responses as a percentage of total touches. Radiant heat test was performed using a device designed for the purpose of identifying heat sensitivity (Paw Thermal Stimulator System, University Anesthesia

Research & Development Group, San Diego, CA, USA). Rats were placed on the temperature-regulated glass platform heated to 30°C, and the lateral plantar surface of the hindpaws were stimulated with a radiant heat source (50 W halogen bulb) directed through an aperture. The time elapsed from initiation of the stimulus until withdrawal (withdrawal latency) as detected by a photocell was measured. Each hindpaw was tested 4 times and the withdrawal latency values averaged.

### *Immunolabeling and analysis*

For immunohistochemistry (IHC), animals tested were terminally anesthetized. L4/5 DRGs, sciatic nerves, and the medial plantar and hairy skin of hindpaws were dissected, postfixed in 10% buffered zinc formalin (ThermoFisher, Pittsburgh, PA, USA), and processed for paraffin embedding and sectioning. IHC double staining was performed to characterize cellular specificity and distribution of target molecules in sections, as previously described.<sup>35</sup> Briefly, 5- $\mu$ m thick sections were de-paraffinized in xylene and rehydrated through graded alcohols and treated by heat-induced epitope retrieval in 10 mM citrate buffer, pH 6.0~7.0 (depending on the antibody used). Sections were first immunolabeled with the selected primary antibodies overnight at 4°C (Table 1). The specificity of a rabbit extracellular TRPA1 antibody (Alomone, Jerusalem, Israel), which recognizes the epitope (NSTGIINETS DHSE) corresponding to amino acid residues 747 to 760 in the first extracellular loop of human TRPA1, has been validated in previous publications for identifying TRPA1 immunopositive profiles in rat and mouse DRGs by the previous publications.<sup>19,36–40</sup> We also tested the specificity by preincubating the antibody solution with the specific TRPA1 antigenic peptides (5  $\mu$ g/ml, Alomone) for 2 hr prior to immunostaining, as described previously.<sup>15</sup> The specificities of the other antibodies used in this study have been previously confirmed.<sup>15,30,41,42</sup> All antibodies were diluted in 1 $\times$  phosphate-buffered saline (PBS), containing 0.05% Triton X-100 and 3% bovine serum albumin. Normal immunoglobulin G (IgG from same species as the first antibody, Table 1) was replaced for the first antibody in negative controls. The appropriate fluorophore-conjugated (Alexa 488 or Alexa 594, 1:2000) secondary antibodies (Jackson ImmunoResearch, West Grove, PA, USA) were used to reveal immune complexes. The sections were washed three times 5 min each with PBS containing 0.05% Tween-20 between incubations. To stain nuclei, 1.0  $\mu$ g/ml Hoechst 33342 (ThermoFisher) was added to the secondary antibody mixture. The sections were examined, and images were acquired on a Nikon TE2000-S fluorescence microscope (El Segundo, CA, USA), equipped with an Optronics QuantiFire digital camera and

**Table 1.** Primary antibodies and IgG controls used in this study.

Ab <sup>a</sup>	Host	Supplier/Cat#/RRID ID <sup>b</sup>	Dilution
TRPA1	Rabbit polyclonal	Alomone/ACC-037/AB2040232	1:200 (IHC), 1:800 (Wb)
Tubb3	Mouse monoclonal	SCB/sc80016	1:200 (IHC), 1:1000 (Wb)
NKA1 $\alpha$	Mouse monoclonal	SCB/sc48345	1:1000 (IHC and Wb)
GFAP	Rabbit polyclonal	Dako/Z0334	1:1000 (IHC and Wb)
GFAP	Mouse monoclonal	CS/3670	1:100 (IHC)
GAPDH	Mouse monoclonal	PT/2555	1:5000 (Wb)
MBP	Goat monoclonal	SCB/sc13912	1:500 (IHC)
S100	Mouse monoclonal	TF/MS296P1	1:800 (IHC)
CK14	Mouse monoclonal	SCB/sc53253	1:200 (IHC)
IgG	Mouse	TF/31903	1:100~400
IgG	Goat	TF/31245	1:500
IgG	Rabbit	TF/MA5-16384	1:200~1000

<sup>a</sup>Antibody abbreviations: TRPA1: transient receptor potential cation channel subfamily A member 1; Tubb3:  $\beta$ 3-tubulin; NKA1 $\alpha$ : sodium/potassium ATPase 1 alpha; GFAP: glial fibrillary acidic protein; GAPDH: glyceraldehyde 3-phosphate dehydrogenase; MBP: myelin basic protein; S100, S-100 calcium-binding protein; CK14: cytokeratin-14; IgG: immunoglobulin G; IHC: immunohistochemistry.

<sup>b</sup>Alomone: Alomone Labs, Jerusalem, Israel; SCB: Santa Cruz Biotechnology, Santa Cruz, CA; Dako: Carpinteria, CA; CS: Cell Signaling Technology, Danvers, MA; PT: Proteintech, Rosemont, IL; TF: ThermoFisher, Waltham, MA.

acquisition software (Ontario, NY, USA), as well as filters suitable for selectively detecting the green, red, and blue fluorescence. For each comparative experiment, all images were acquired with identical settings for detector gain and capture time under a 10 $\times$  objective (0.5 numerical aperture at 2048  $\times$  2048 pixel resolution) or 20 $\times$  objective (0.3 numerical aperture at 1024  $\times$  1024 pixel resolution). Some IHC images were captured using a Nikon C1 digital eclipse confocal microscope (Nikon). For double-label colocalization, images from the same section but showing different antigen signals were overlaid.

Intensity correlation analysis (ICA) was performed to determine colocalization of TRPA1 with neuronal plasma membrane (PM) marker sodium/potassium-ATPase 1 $\alpha$  (NKA1 $\alpha$ ) and SGC marker glial fibrillary acidic protein (GFAP) as previously described using ImageJ 1.46r software plugin (<http://imagej.nih.gov/ij>).<sup>15,43</sup> Briefly, fluorescence intensity was quantified in matched regions of interest (the green and red colors varied in close synchrony) for each pair of images. Mean background was determined from areas outside the section regions and was subtracted from each file. On the basis of the algorithm, in an image where the intensities vary together, the product of the differences from the mean (PDM) will be positive, which shows as skewing to right when this relationship is plotted, and represents colocalization of the two antigens. If the pixel intensities vary asynchronously (the channels are segregated, indicating absence of costaining), then most of the PDM will be negative. The intensity correlation quotient (ICQ) is based on the nonparametric sign-test analysis of the PDM values and is equal to the ratio of the number of positive PDM values to the total number of pixel

values. The ICQ values are distributed between  $-0.5$  and  $+0.5$  by subtracting 0.5 from this ratio. In random staining, the ICQ approximates 0. In segregated staining, ICQ is less than 0, while for dependent staining, ICQ is greater than 0.<sup>15,43</sup>

### *DRG dissociated cell culture and neuron-free SGC culture*

The L4/5 DRG were rapidly harvested from the isoflurane-anesthetized animals and were incubated in 0.01% blendzyme 2 (Roche Diagnostics, Madison, WI, USA) for 30 min followed by incubation in 0.25% trypsin and 0.125% DNase for 30 min, both dissolved in Dulbecco's modified Eagle medium/F12 with glutaMAX (ThermoFisher). After exposure to 0.1% trypsin inhibitor and centrifugation, the pellet was gently triturated in culture medium containing neural basal media A (ThermoFisher) plus 0.5  $\mu$ M glutamine. A time-differential attachment protocol for astrocyte isolation was adapted to establish neuron-free SGC culture.<sup>44</sup> Initially, the dissociated DRG cells were plated on culture dishes for 4 hr for SGC attachment, and then neurons that grow loosely attached to the top of mixed cultures were separated by hand-shaking of the culture flasks gently for 5 to 10 min or at 100 r/min on a gyratory shaker, followed by replacing with new cultural medium. The attached glial cells were cultured in the medium containing 10% fetal bovine serum to promote cell division while inhibiting differentiation thereby increasing cell numbers. To initiate SGC differentiation after 2 to 6 days in vitro (DIV), the cultures were switched to a serum-free neural basal medium A.



Immunocytochemistry (ICC) of TRPA1 expression was performed on the cultures dissociated from rats and mice as described previously.<sup>30</sup> Dissociated DRG cells cultured for 5 hr and the neuron-free SGC culture were fixed in 2% paraformaldehyde for 10 min. Fixed cells were processed for immunolabeling with a rabbit TRPA1 (1:200) and a rabbit GFAP (1:1000) or a mouse Tubb3 (1:2000) antibodies at 4°C for overnight, followed by the appropriate fluorophore-conjugated secondary antibodies. After immunostaining and washing, the coverslips were mounted onto glass slides for microscopic observation as above. To construct profile size distribution histograms of neurons and SGCs 5 hr after establishment of DRG-dissociated culture, double-labeling ICC was performed using TRPA1 with pan-neuronal marker Tubb3 or SGC-marker GFAP; the diameter and area of marker-labeled cells for which nuclei were evident was measured using Adobe Photoshop CS6 (Adobe Systems Incorporated, San Jose, CA, USA). Neurons were divided into three size groups (rat): small (<700  $\mu\text{m}^2$ ), medium (700–1500  $\mu\text{m}^2$ ), and (>1500  $\mu\text{m}^2$ ) neurons as described previously.<sup>42,45</sup>

### Microfluorimetric $\text{Ca}^{2+}$ imaging

Determination of intracellular  $\text{Ca}^{2+}$  concentration ( $[\text{Ca}^{2+}]_i$ ) was performed using Fura-2-based microfluorimetry and imaging analysis as previously described,<sup>46</sup> with some minor modifications. Growth factors were not added to the media because adult DRG neurons do not require growth factors for survival.<sup>47</sup> Dissociated cells were plated onto 5% laminin-coated glass coverslips (ThermoFisher) and maintained at 37°C in humidified 95% air and 5%  $\text{CO}_2$  for 3 hr and were studied by  $\text{Ca}^{2+}$  imaging no later than 6 hr after harvest. Unless otherwise specified, the agents were obtained from Sigma-Aldrich. For these experiments, neurons were categorized as either large (>45  $\mu\text{m}$  diameter) or small/medium ( $\leq 45 \mu\text{m}$ ). For these experiments, SGCs and small/medium neurons, which include the nociceptor category, were evaluated for responses to the TRPA1-selective agonist allyl isothiocyanate (AITC).

For measurement of  $[\text{Ca}^{2+}]_i$ , dissociated DRG cells cultured on coverslips were loaded with Fura-2-AM (5  $\mu\text{M}$ , ThermoFisher) and maintained in 25°C Tyrode's solution containing (in mM): NaCl 140, KCl 4,  $\text{CaCl}_2$  2, glucose 10,  $\text{MgCl}_2$  2, and 4-(2-hydroxyethyl)-1-piperazineethanesulfonic acid (HEPES) 10, with an osmolarity of 297 to 300 mOsm and pH 7.4. After 30 min, they were washed three times with regular Tyrode's solution and left in a dark environment for de-esterification for 30 min and then mounted onto the recording chamber. In some experiments, a nominally  $\text{Ca}^{2+}$ -free bath solution was used that contained the following (in mM): NaCl 140, KCl 4, glucose 10,  $\text{MgCl}_2$  2,

HEPES 10, and Ethylene glycol-bis(2-aminoethylether)-N,N,N',N'-tetraacetic acid (EGTA) 0.2, producing a calculated  $\text{Ca}^{2+}$  of <1 nM. The 0.5 ml recording chamber was constantly superfused by a gravity-driven bath flow at a rate of 3 ml/min. Agents were delivered by directed microperfusion controlled by a computerized valve system through a 500- $\mu\text{m}$ -diameter hollow quartz fiber 300  $\mu\text{m}$  upstream from the chamber. This flow completely displaced the bath solution, and constant flow was maintained by delivery of bath solution when specific agents were not being administered. Solution changes were achieved within 200 ms. The fluorophore was excited alternately with 340 nm and 380 nm wavelength illumination (150 W xenon, Lambda DG-4; Sutter), and images were acquired at 510 nm using a cooled 12 bit digital camera (Coolsnap fx; Photometrics, Tucson, AZ, USA) and inverted microscope (Diaphot 200; Nikon) through a 20 $\times$  or 40 $\times$  Fluor oil-immersion objective.  $[\text{Ca}^{2+}]_i$  was evaluated as the ratio of emission in response to excitation at 340 and 380 nm, expressed as the 340/380 nm fluorescence emission ratio ( $R_{340/380}$ ) that is directly correlated to the amount of intracellular calcium.<sup>46</sup> A  $\geq 30\%$  increase in  $R_{340/380}$  from baseline after superfusion with AITC was considered a positive response<sup>48</sup> for both neurons and SGCs. Response of neurons to 50 mM KCl solution at the end of each protocol was used as a criterion for identifying viable neurons, and similarly for the response of SGCs to 10  $\mu\text{M}$  ATP. PM  $\text{Ca}^{2+}$ -ATPase influence was eliminated by applying Tyrode's with pH 8.8 during depolarization, while stable cytoplasmic  $[\text{Ca}^{2+}]_c$  was maintained by simultaneously reducing bath  $\text{Ca}^{2+}$  concentration to 0.25 mM.<sup>49</sup>

### Immunoblots

The lysates from DRG tissues and cultured cells were extracted using 1 $\times$  radioimmunoprecipitation assay buffer (20 mM Tris-HCl pH 7.4, 150 mM NaCl, 1% Nonidet P-40, 1% sodium deoxycholate, 0.1% sodium dodecyl sulfate, with 0.1% Triton X100 and protease inhibitor cocktail). To examine the subcellular localization of TRPA1, DRG tissues were fractionated to obtain PM fractions enriched in NKA1 $\alpha$ , and cytosol fractions lacking NKA1 $\alpha$ , using the ProteoExtract Subcellular Proteome Extraction Kit (ThermoFisher), which contains extraction buffers with ultrapure chemicals to ensure high reproducibility, protease inhibitor cocktail to prevent protein degradation, and benzonase nuclease to remove contaminating nucleic acids, according to the manufacturer's instructions. Protein concentration was determined by using the Pierce BCA kit (ThermoFisher). Equivalent protein samples were size separated using 4% to 20% or 10% sodium dodecyl sulfate-polyacrylamide gel electrophoresis gels (Bio-Rad Laboratories, Des

Plaines, IL, USA), transferred to 0.22  $\mu$ m polyvinylidene difluoride membranes, and blocked for 1 hr in 5% skim milk. The blots were cut into high (>70 KDa), medium (50–70 KDa), and low (>50 KDa) protein-size strips or two halves along protein size around 70 KDa<sup>50</sup> and then subsequently incubated overnight at 4°C with a rabbit anti-TRPA1 (1:400, 100~130 KDa), a mouse monoclonal anti-NKA1 $\alpha$  (1:1000, ~100 KDa), a mouse monoclonal anti-tubb3 (1:1000, ~55 KDa), and a mouse monoclonal anti-glyceraldehyde 3-phosphate dehydrogenase (GAPDH) (1:5000, ~37 KDa). To verify the band specificity of TRPA1 detection using a rabbit TRPA1 antibody, the antibody solution was preincubated with the specific TRPA1 antigenic peptides (5  $\mu$ g/ml, Alomone) for 2 hr prior to immunoblotting. Immunoreactive proteins were detected by Pierce enhanced chemiluminescence (ThermoFisher) on a ChemiDoc Imaging System (Bio-Rad) after incubation for 1 hr with horseradish peroxidase-conjugated second antibodies (1:5000, Bio-Rad). Densitometry of bands of interest was analyzed using ImageJ v.1.46. Ratios of the band density of the target protein to the sum of house-keeping genes (Tubb3 or GAPDH) and NKA1 $\alpha$  band density were calculated and the percentage changes of target protein in the experimental samples compared with those from the control samples.<sup>51,52</sup>

### Reverse transcription polymerase chain reaction

Total RNA was extracted from DRG tissue and purified neuron-free SGCs cultured 4 DIV using RNAeasy kit (Qiagen, Carlsbad, CA, USA) and then treated with DNase I (Life Technologies). Complementary DNA (cDNA) was synthesized from 1.0  $\mu$ g RNA using the Superscript III first strand synthesis kit with random hexamer primers (Life Technologies). Polymerase chain reaction (PCR) was carried out on a Bio-Rad C1000 PCR Machine and specific intron-spanning primers from rat TRPA1 (forward 5'-ATGGCACC CCTTACATAGC-3' and reverse 5'-GGCCATGC ATTTGGCATTCT-3'). The thermal cycling conditions were one cycle at 95°C for 3 min, 40 cycles at 95°C for 10 s, 60°C for 30 s, and 68°C for 1 min, followed by one cycle at 72°C for 5 min. This generated a single band (437 bp) for the rat TRPA1. PCR products were gel extracted and sequence analyzed by Retrogen (San Diego, CA, USA).

### Statistics

Statistical analysis was performed with GraphPad PRISM 6 (GraphPad Software, San Diego, CA, USA). Behavioral changes over baseline and between groups for von Frey and heat measurements were generated using repeated measures two-way analysis of variance

(ANOVA) and post hoc analysis with Bonferroni test. Pin test results in discrete numerical data without normal distribution, so conservative nonparametric analysis was performed by Friedman's test for ANOVA and Dunn's test for post hoc analysis. The differences of the targeted gene expression by immunoblots and calcium imaging analysis were compared with one-way ANOVA, two-tailed unpaired *t*-test, or Mann-Whitney test, where appropriate. Results are reported as mean and standard deviation of mean. Significances of ICQs of TRPA1 immunocolocalization with NKA and GFAP were analyzed by means of the normal approximation of the nonparametric Wilcoxon rank test (sign test), as described previously.<sup>43,52</sup> The value  $p < 0.05$  was considered statistically significant.

## Results

### *TRPA1 is expressed in primary sensory neurons, SGCs, and SCs in the adult rat*

Various anti-TRPA1 antibodies have been used to detect TRPA1 expression by IHC and immunoblot. In this study, we chose a rabbit extracellular TRPA1 antibody for several reasons: (1) this antibody has been well characterized by the vendor, demonstrating a high specificity against an epitope (NSTGIINETS DHSE) corresponding to amino acid residues 747 to 760 in the first extracellular loop of TRPA1 (Figure 1a); (2) the specificity has been verified in TRPA1 knockout tissue;<sup>38</sup> and (3) it consistently detects TRPA1 expression by IHC or immunoblot from DRGs and from nonneuronal tissues.<sup>19,36–38,40,53–63</sup> We also tested the specificity of this antibody in the detection of TRPA1 expression. By immunoblot, the antibody revealed a clean band at ~120 KDa as the target protein in the homogenates of the DRGs from adult rats, and preincubation with excess immunogenic peptide completely eliminated the band (Figure 1b). An additional band at ~50 KDa was occasionally detected, which probably resulted from the proteolytic cleavage of the target protein either naturally or generated during sample preparation, since it can be blocked by immunogenic peptide preabsorption and is not always present (e.g. see Figure S1). TRPA1 immunoreactivity (IR) displayed ring-like profiles in DRG sections, in a pattern that could represent TRPA1 immunopositivity in neuronal membrane, perineuronal SGCs, or both, and this TRPA1-IR was blocked by preincubation with excess immunogenic peptide (Figures 1c, c1, d, and d1). We further verified the specificity of TRPA1 detection with this antibody by immunolabeling DRG sections and DRG dissociated cultures from TRPA1 knockout mice. These samples lacked the characteristic staining mentioned above that was present in wild-type littermates

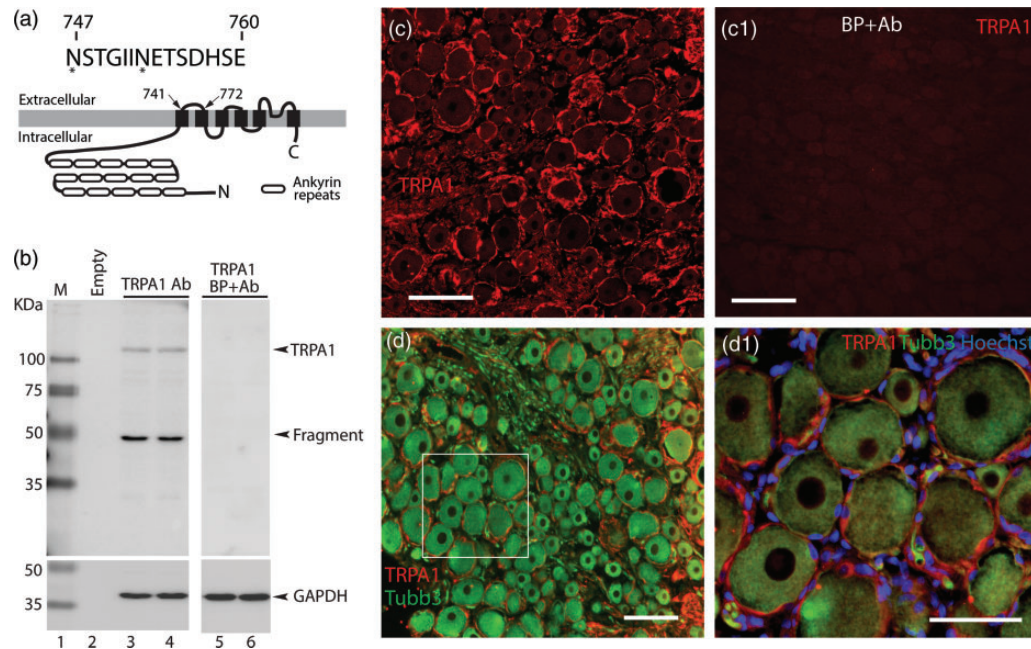


**Figure 1.** Specificity evaluation of TRPA1 antibody. Schematic diagram (a) illustrates TRPA1 topology structure, with the amino acid sequence of the antigenic peptide shown at the top of the panel. Stars below asparagine (N) at the first and seventh position of the peptide indicate the potential glycosylation sites. Immunoblot revealed a clean band around  $\sim 120$  KDa of TRPA1, with an additional band around  $\sim 50$  KDa, in the homogenates of rat DRG, and preincubation with excess immunogenic peptide completely eliminated both bands (b). TRPA1 was detected by IHC in rat DRG sections as a ring profile (c), and the label was eliminated by preabsorption of the antibody with an excess of the antigenic BP (c1). Representative images of double immunostaining of TRPA1 (red) and Tubb3 (green) showed that a large proportion of TRPA1 immunoreactivity (IR) encircles Tubb3-labeled neurons (d). The area within the white square in (d) is shown at higher magnification in (d1). Scale bars:  $100 \mu\text{m}$  for all.

TRPA1: transient receptor potential cation channel subfamily A member 1; GAPDH: glyceraldehyde 3-phosphate dehydrogenase; Tubb3:  $\beta 3$ -tubulin; BP: blocking peptide.

(Figure S2). These results confirm that this antibody against an extracellular epitope of TRPA1 is likely specific for detecting the target in rat DRG tissues by both IHC and immunoblot.

To identify whether the profile of TRPA1 expression encircling the neurons consists of expression in neuronal PM or surrounding SGCs, we performed double immunolabeling of TRPA1 with GFAP, a SGC signature marker, or sodium/potassium ATPase 1 alpha ( $\text{NKA1}\alpha$ ), a canonical neuronal PM marker. Double immunolabeling of GFAP with  $\text{NKA1}\alpha$  demonstrated the specificity of GFAP labeling SGCs and  $\text{NKA1}\alpha$  staining neuronal membrane (Figure S3). Overlaid images of TRPA1 with GFAP showed clear colocalization of two immunopositivity (Figure 2a and b), and the ICA plots of TRPA1 and GFAP were strongly skewed toward positive values (Figure 2c), consistent with colocalization in SGCs, and the ICQ value was positive ( $0.366$ ,  $p_{\text{sign test}} < 0.001$ ). Overlaid images of TRPA1 with  $\text{NKA1}\alpha$  and pixel intensity line-plot profiles of cross-sections clearly identified a portion of TRPA1 as neuronal PM localization (Figures 2d to d2, e, and f). ICA plots of TRPA1 and  $\text{NKA1}\alpha$  were strongly skewed

toward positive values with the calculated ICQ value of  $0.333$  ( $p_{\text{sign test}} < 0.001$ ) (Figure 2g), consistent with colocalization. These data thus suggest that at least a portion of the TRPA1 expression around the neurons is within the neuronal PM and that antibody-detected TRPA1 expression is localized to both the primary sensory neurons and the perineuronal SGCs. Neuronal and SGC expression of TRPA1 was also confirmed by ICC labeling of TRPA1 on acutely dissociated DRG cultures (5 hr) (Figure 2h to h2). In the neuron-free and SGC-enriched cultures (Figure 2i), ICC showed high immunopositive for TRPA1 and GFAP (Figure 2j to j2). Reverse transcription polymerase chain reaction (RT-PCR)-amplified TRPA1 cDNA from SGCs were verified by sequencing analysis (Figure 2k), and Western blot detected TRPA1 positivity on the lysate of these cells (Figure 2l), adding further evidence for the presence of TRPA1 in SGCs.

TRPA1 has been reported to be expressed by the SCs.<sup>23</sup> Our double-labeling data showed a high degree of colabeling with antibodies for TRPA1 and S100 (a marker positive for both SGCs as well as myelinating and nonmyelinating SCs) in the perisomatic SGCs of



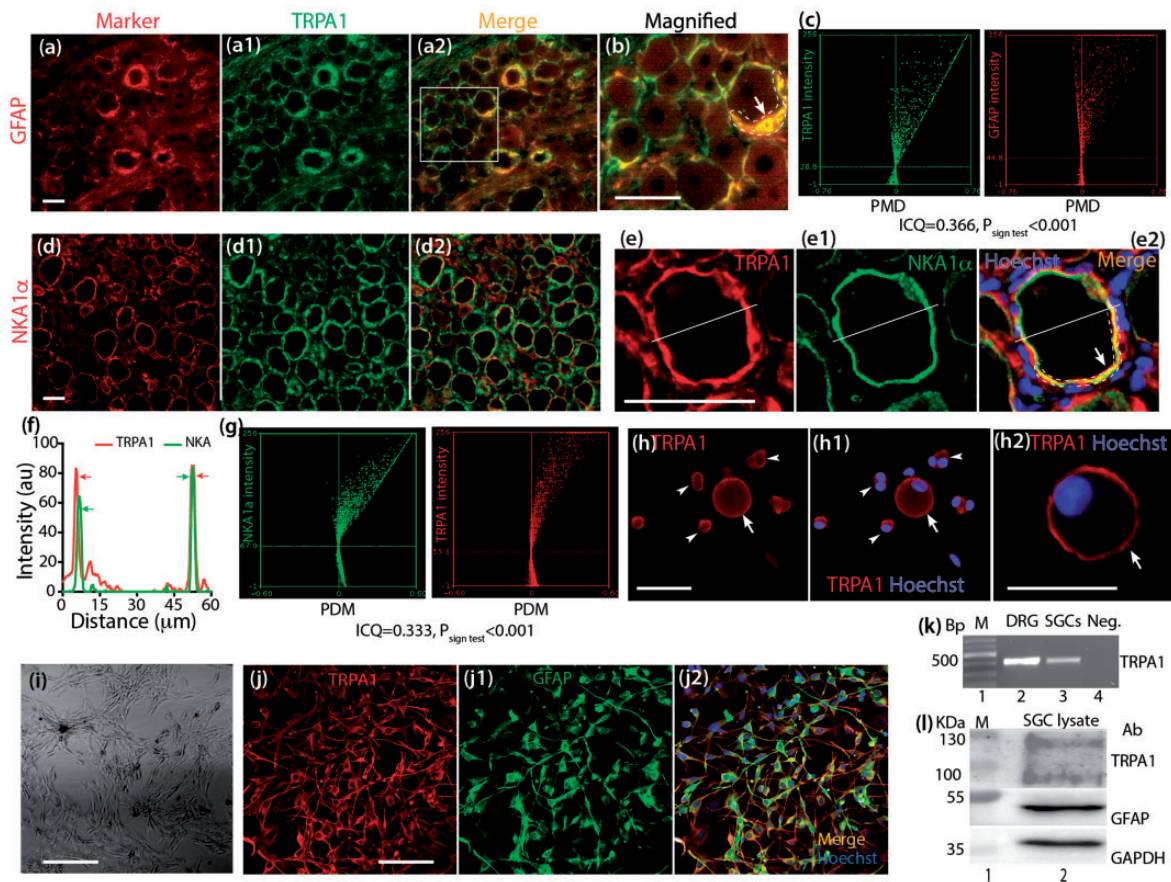


**Figure 2.** IHC delineation of TRPA1 localization to primary sensory neurons and SGCs. Representative montage images show immunostaining of TRPA1 (green) with SGC marker GFAP (red), showing colabeling (yellow) in the merged image (a–a2). The area within the white square in (a2) is shown at higher magnification in (b). ICA colocalization (see Materials and Methods section) of a demarked area (b, white dashed line, arrow) produces scatter plots of intensity versus PDM (c) that show strong right skewing for TRPA1 and GFAP, with an ICQ value of 0.366 ( $p_{\text{sign test}} < 0.001$ ), indicating immunocolocalization. Representative montage images (d–d2) show immunostaining of TRPA1 (green) and a canonical neuronal PM marker NKA1 $\alpha$  (red), as well as colabeling (yellow). A cell profile (e–e2) analyzed for pixel intensity (f) along a cross-section (lines in e–e2) shows a clear overlap of TRPA1 (red) and NKA1 $\alpha$  (green) on the right cell margin (right side peak), indicating TRPA1 localized in the plane of the PM (e2, arrow). Scatter plots (g) for the region enclosed by the white dashed line (arrow in panel e2) show strong right skewing for NKA1 $\alpha$  and TRPA1 resulting in an ICQ of 0.333 ( $p_{\text{sign test}} < 0.001$ ), indicating immunocolocalization. ICC on primary cultures 5 hr after DRG dissociation (h–h2, arrows denote neurons and arrowheads point to SGCs) show neuronal and SGC TRPA1 immunopositivity with a profile of membrane localization. Neuron-free primary SGC culture established 18 hr after dissociation (i) shows a majority of cells fully differentiated and positive for TRPA1 and GFAP by ICC (j–j2), and TRPA1 was detected by RT-PCR (k) and immunoblot in the lysate of these cells (l). Scale bars: 50  $\mu\text{m}$  for all.

TRPA1: transient receptor potential cation channel subfamily A member 1; GFAP: glial fibrillary acidic protein; PDM: product of the differences from the mean; ICQ: intensity correlation quotient; NKA1 $\alpha$ : sodium/potassium ATPase I alpha; DRG: dorsal root ganglia; SGC: satellite glial cell; GAPDH: glyceraldehyde 3-phosphate dehydrogenase.

DRG sections (Figure 3a), and in the SCs of sciatic nerve sections (Figure 3b to b2), but no TRPA1 costaining with myelin basic protein (MBP) (Figure 3c, 3d to d2), which is a major constituent of periaxonal myelin laminae and a myelinating SC marker.<sup>64</sup> These results indicate that TRPA1 is expressed in the nonmyelinating SCs that also are a component of the perineuronal glial cell population and that comprise the majority of the nucleated cells in the peripheral nerve trunk.<sup>65</sup> Additionally, consistent with a previous report,<sup>66</sup> we

also detected TRPA1-IR in the various cutaneous primary afferent terminal structures in the rat hindpaw skin sections (Figure 3e to j).

### SGCs possess functional TRPA1

Imaging the response of  $[\text{Ca}^{2+}]_i$  to TRPA1 activation is a useful approach for determining functional expression of TRP receptors.<sup>47,67</sup> In order to distinguish neurons and SGCs, we first sought to determine if small soma size



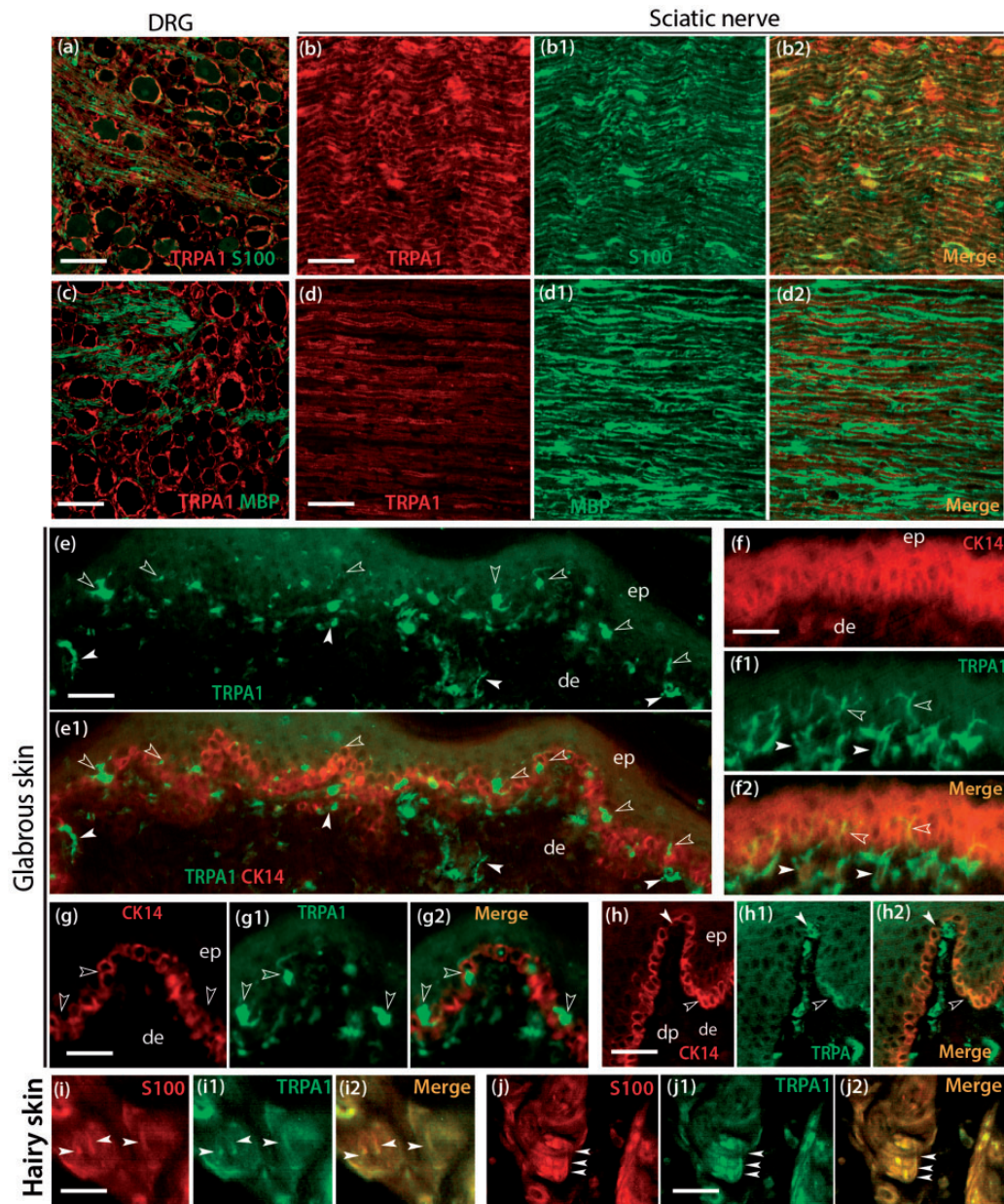


**Figure 3.** IHC delineation of TRPA1 expression in Schwann cells (SCs) and skin afferent terminals. Representative image (a) shows double labeling of TRPA1 (red) with S100 (green), a nonmyelinating SC marker, in DRG section, delineating colocalized TRPA1 and S100 immunopositivity in perineuronal glial cells and nerve fibers within the section. Representative sciatic nerve montage images of TRPA1 immunostaining (b) with S100 (b1) show high colocalization (b2), but minimal colocalization of TRPA1 with MBP, a marker of myelinating SCs, was evident in DRG section (c) and sciatic nerves (d–d2). (Weak staining of S100 in neuronal somata is also observed, likely representing nonspecific reaction.) Representative images of hindpaw glabrous skin sections (e–h) show TRPA1 IHC (green), costained with a CK14 antibody that selectively labels the epidermal stratum basal layer (red) for identifying the epidermis (ep) and dermis (de); empty and filled arrowheads identify structures in epidermis and dermis, respectively. TRPA1 immunopositivity is identified in various cutaneous primary afferent terminal structures (e, e1), suggestive of epidermal and dermal terminal neuronal fibers (f–f2), intraepidermal Merkel cells within the basal layer of the epidermis and their fibers (g–g2), and Meissner’s corpuscles in the dermal papillae bulge area of hindpaw glabrous skin (h–h2). TRPA1-IR costained with S100 was also observed in the lanceolate endings (i–i2 and j–j2, arrowheads) in palisades around hair follicle of hindpaw dorsal hairy skin. Scale bars: 100  $\mu\text{m}$  for all.

DRG: dorsal root ganglia; TRPA1: transient receptor potential cation channel subfamily A member 1; MBP: myelin basic protein; CK14: cytokeratin-14.

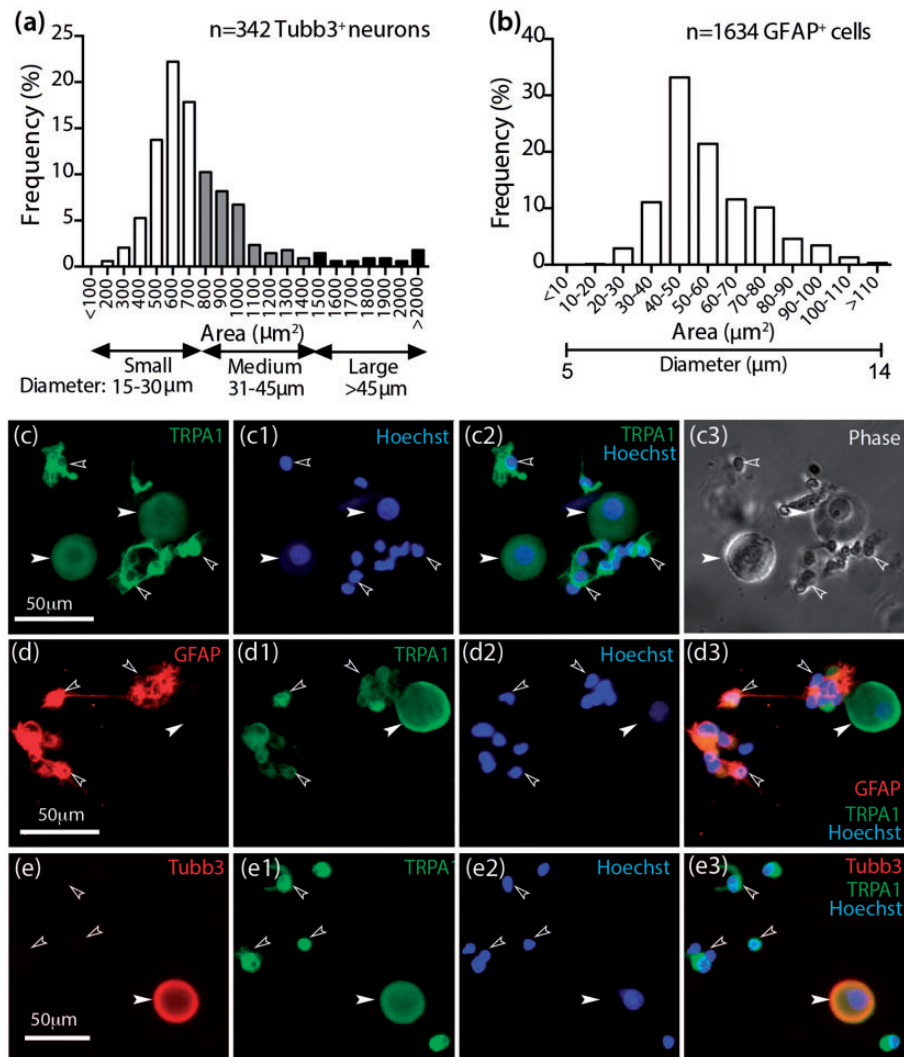


**Figure 4.** Size frequency distribution of neurons and SGCs in acute DRG dissociated culture. Histograms show the frequencies of somata sizes of tubb3-positive neurons (a,  $n=342$ ) and GFAP-positive SGCs (b,  $n=1734$ ) 5 hr after lumbar DRG dissociation. ICC shows immunopositivity for TRPA1 (c–c3), double immunolabeling with the GFAP (d–d3) that stains SGCs as well as nonmyelinating Schwann cells, and double immunolabeling with the pan-neuronal marker Tubb3 (e–e3). The filled and empty arrowheads identify neurons and SGCs, respectively. Scale bars are 50  $\mu\text{m}$  for all images.

GFAP: glial fibrillary acidic protein; Tubb3:  $\beta$ 3-tubulin; TRPA1: transient receptor potential cation channel subfamily A member 1.

could be used as a proxy to identify SGCs as distinct from neurons in cultures of acutely dissociated DRG cells. Accordingly, we characterized the size frequency distribution of immunolabeled Tubb3<sup>+</sup>-neurons and GFAP<sup>+</sup>-SGCs at 5 to 6 hr after establishment of cells dissociated from L4 and L5 DRG obtained from 8 naïve rats at 6 to 8 weeks old. Results (Figure 4a and b) showed that the large majority (>95%) of neuron somata in cultures are small and medium in size with average diameter around 20 to 32  $\mu\text{m}$  and that no neuron was smaller than 15  $\mu\text{m}$  diameter (area 110  $\mu\text{m}^2$ ). The large majority (>95%) of nonneuronal cells (SGCs and SCs) in the cultures (size <15  $\mu\text{m}$ ) were GFAP positive, identifying them as SGCs (including

nonmyelinating SCs). The size range of this population is from 5 to 15  $\mu\text{m}$  diameter (10~110  $\mu\text{m}^2$ ). Colabeling of TRPA1 with a pan-neuronal marker Tubb3 or SGC marker GFAP verified correct identification of neurons versus glial cells (Figure 4c to e). Thus, there was minimal overlap of neurons (<110  $\mu\text{m}^2$ ) with GFAP<sup>+</sup>-SGCs (>110  $\mu\text{m}^2$ ) in the dissociated cultures in our experiment, which allowed subsequent identification of neurons and SGCs by somatic size alone.

To activate TRPA1, we used AITC, a commonly used selective agonist. A  $\geq 30\%$  increase in  $R_{340/380}$  over baseline (i.e.  $\Delta R_{340/380}$ ) during AITC superfusion (100  $\mu\text{M}$ , 1 min) was observed in both neurons and SGCs, although AITC-evoked  $[\text{Ca}^{2+}]_i$  rise in SGCs is much

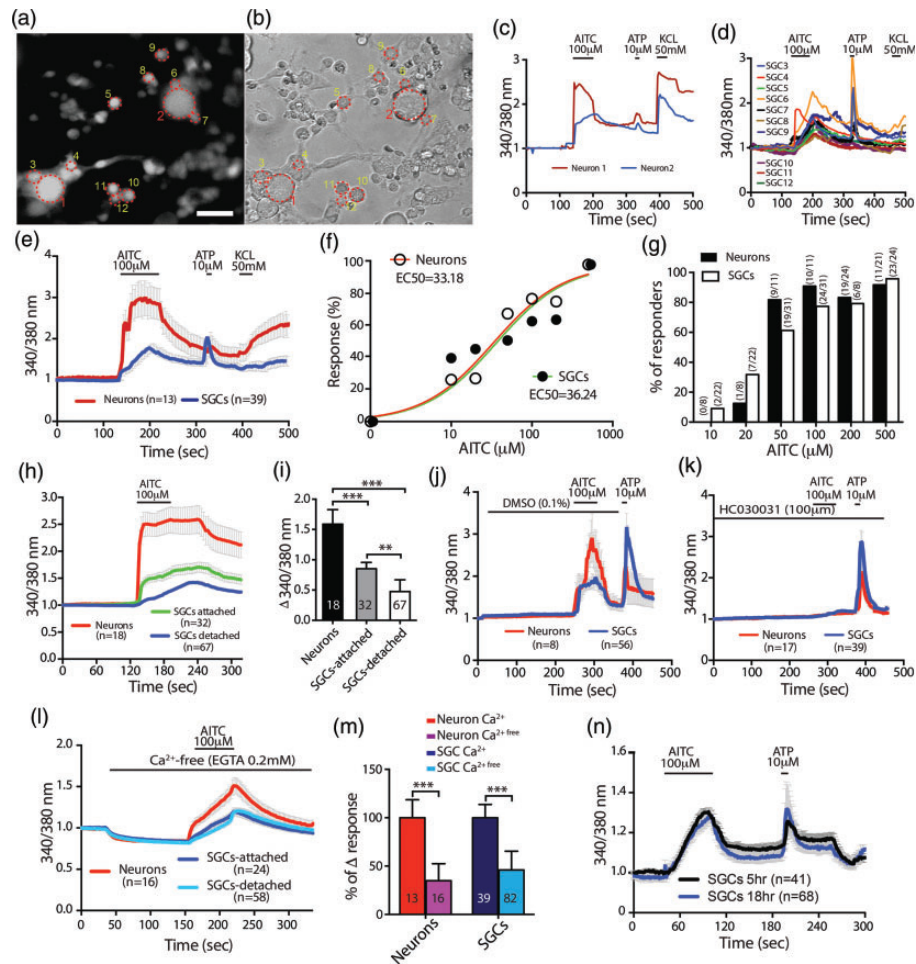


**Figure 5.** AITC-evoked calcium transients in neurons and SGCs of DRG dissociated cultures. Representative fluorescent and phase images show cultured sensory neurons and glial cells loaded with Fura-2/AM, with numbers aside the examples of neurons and SGCs encircled by red dashed lines (a, b). Scale bar, 40  $\mu\text{m}$ . The  $[\text{Ca}^{2+}]_i$  rise over baseline after 1 min superfusion of AITC (100  $\mu\text{M}$ ), sequentially challenged with ATP (10  $\mu\text{M}$ ) and KCl (50 mM) in normal  $\text{Ca}^{2+}$  conditions, was measured in the representative neurons (c) and SGCs (d) encircled in panel (a). The averaged traces of neurons and SGCs recorded evoked by 100  $\mu\text{M}$  AITC were compared between neurons and SGCs (e). Concentration–response curves of AITC-evoked increases of  $[\text{Ca}^{2+}]_i$  (f) and the response rates for neurons and SGCs (g) are shown. The dots in panel (f) represent mean values of percentage of  $[\text{Ca}^{2+}]_i$  at each dose normalized to maximal response of 500  $\mu\text{M}$  AITC (empty dots are neurons; black dot are SGCs). The EC50 of neuron and SGC to AITC activation is indicated. The numbers on each bar of panel (g) represent the responders versus total cells adhesive and recorded at different AITC concentration. AITC-evoked  $[\text{Ca}^{2+}]_i$  increases in the attached SGCs were significantly higher than the detached SGCs (h and i, the numbers in each bar denotes the cells recorded.  $**p < 0.01$  and  $***p < 0.001$ , one-way ANOVA, Tukey post hoc analysis). Dimethyl sulfoxide (0.1%, the solvent used to dissolve AITC) had no effect on  $[\text{Ca}^{2+}]_i$  (j). The AITC-evoked  $[\text{Ca}^{2+}]_i$  increase was completely blocked by the TRPA1 antagonist HC-030031 (100  $\mu\text{M}$ ) in both neurons and SGCs (attached and detached combined for this analysis) (k). Increase in  $[\text{Ca}^{2+}]_i$  by AITC (100  $\mu\text{M}$ ) persisted in  $\text{Ca}^{2+}$ -free conditions (l, m,  $***p < 0.001$ , two-tailed unpaired Student's *t*-tests). No significant difference was observed for the isolated SGCs from naïve DRG in response to AITC (100  $\mu\text{M}$ ) between 5 hr and 18 hr (n), which show similar responses to AITC (100  $\mu\text{M}$ ) of SGCs to those exposed to AITC (100  $\mu\text{M}$ ) in the presence of neurons. AITC: allyl isothiocyanate; SGC: satellite glial cell; EC50: half maximal effective concentration; DMSO: dimethyl sulfoxide.

smaller than the response in neurons (Figure 5a to e). The magnitude of  $\Delta R_{340/380}$  in neurons upon 100  $\mu\text{M}$  AITC application showed  $2.407 \pm 0.45$  fold higher over baseline, while SGCs were  $0.87 \pm 0.12$  fold higher over baseline. We note that cultured SGCs are minimally responsive to KCl (Figure 5d). The concentration–response curves of AITC-evoked increases of  $[\text{Ca}^{2+}]_i$  generated by nonlinear regression of  $\Delta R_{340/380}$  across a

range of AITC concentrations (1 to 500  $\mu\text{M}$ ) in neurons and SGCs dissociated from L4/L5 DRG of naïve rats showed similar concentration-dependent responses in both cell types (Figure 5f). The half maximal effective concentrations (EC50) for AITC were comparable (33.18  $\mu\text{M}$  for neurons and 36.24  $\mu\text{M}$  for SGCs). SGCs showed more responders than neurons to AITC at low dose range (Figure 5g). Using 100  $\mu\text{M}$  AITC, 78% (70/



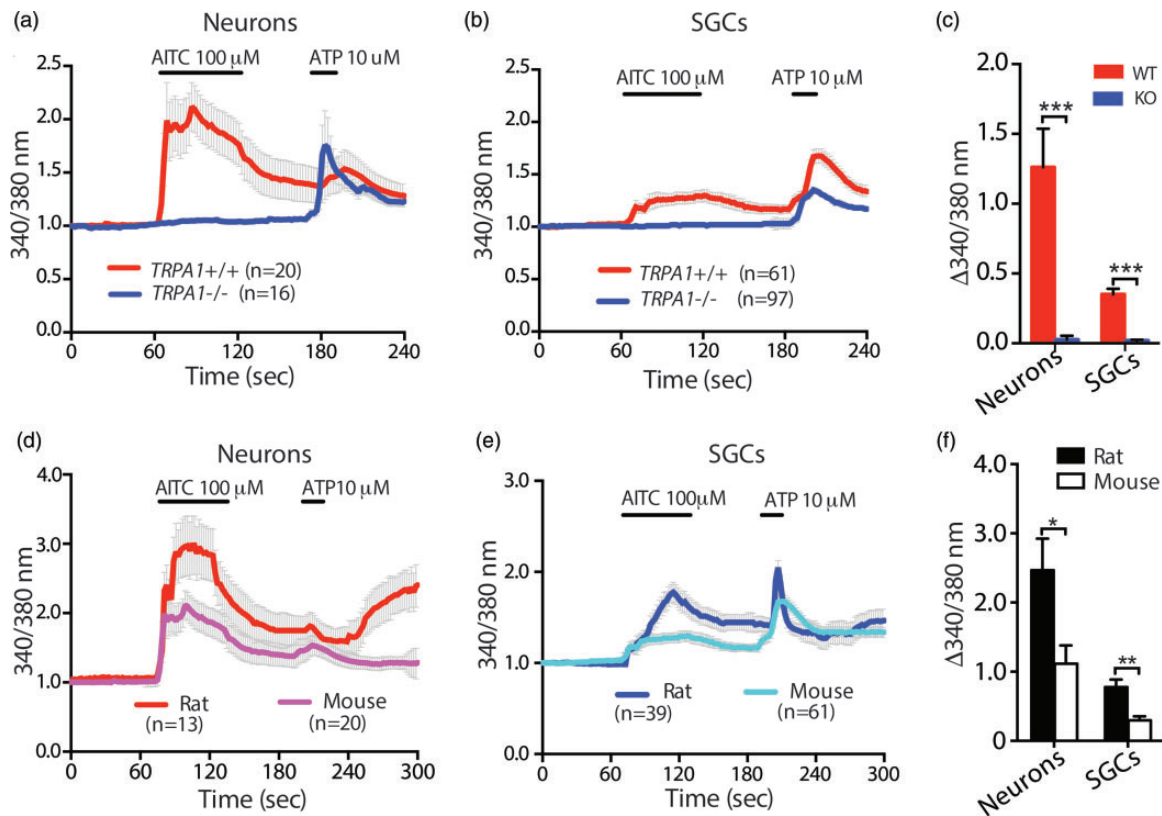


**Figure 6.** Species difference of SGC-TRPA1 derived calcium transients between rat and mouse. Both neurons (a) and SGCs (b) show increased  $[Ca^{2+}]_i$  during AITC (100  $\mu$ M) superfusion in *TRPA1*<sup>+/+</sup> mouse DRG culture, but there was no  $[Ca^{2+}]_i$  response in the neurons (a) nor SGCs (b) from *TRPA1*<sup>-/-</sup>, as summarized in (c) ( $n=4$  animals for both genotypes). AITC-evoked  $[Ca^{2+}]_i$  responses in *TRPA1*<sup>+/+</sup> mouse neurons and SGCs are smaller than those recorded from rat cells (d-f). Note that mouse traces in (d) and (e) are the same data as the *TRPA1*<sup>+/+</sup> traces in (a) and (b). \* $p<0.05$ , \*\* $p<0.01$ , and \*\*\* $p<0.001$  (unpaired, two-tailed Student's *t*-test).

AITC: allyl isothiocyanate; SGC: satellite glial cell; TRPA1: transient receptor potential cation channel subfamily A member 1; WT: wild type; KO: knockout.

90) of total neurons recorded responded to stimulation. Smaller-sized neurons showed higher rate and magnitude of response to 100  $\mu$ M AITC (Figure S4), as previously reported.<sup>47</sup> For SGCs, 72% (228/317) of totally recorded SGCs responded to 100  $\mu$ M AITC. We separately analyzed responses of SGCs according to whether the SGCs remained attached to neurons or were independent of neurons, which showed that attached SGCs developed greater responses to AITC than those that were entirely isolated (Figure 5h, i), although we cannot distinguish whether this is due to an optical contribution from the neurons to which the recorded SGCs was attached, versus a neuron-SGC interaction that results in an amplified  $Ca^{2+}$  response, such as a  $Ca^{2+}$  wave propagating from the neuron to neighboring cells.<sup>68,69</sup> Finally, the  $Ca^{2+}$  response evoked in both neurons and SGCs by 100  $\mu$ M AITC stimulation was completely blocked by the selective TRPA1 antagonist HC-030031 (Figure 5j and k), supporting the specific dependence of these  $[Ca^{2+}]_i$  events upon TRPA1.

Because both  $Ca^{2+}$  influx and internal  $Ca^{2+}$  release could contribute to the  $[Ca^{2+}]_i$  transients elicited by TRPA1 activation,<sup>46,70</sup> we next investigated to what extent  $Ca^{2+}$  release from internal stores contributed to the response to TRPA1 by measuring  $[Ca^{2+}]_i$  during TRPA1 activation in nominally  $Ca^{2+}$ -free extracellular solution (calculated  $[Ca^{2+}] < 1$  nM). Response to 100  $\mu$ M AITC under these conditions resulted in a diminished  $Ca^{2+}$  response in both neurons and SGCs (Figure 5l), which recovered rapidly on restoration of bath  $Ca^{2+}$  to normal condition.<sup>46</sup> These data show that release of  $Ca^{2+}$  from internal stores accounts for approximately 30% to 40% of the overall  $[Ca^{2+}]_i$  increase upon TRPA1 channel activation using 100  $\mu$ M AITC in both neurons and SGCs (Figure 5m), although this may also include a component from activation of voltage-gated  $Ca^{2+}$  channels. To test the possibility that neuron-to-SGC communication might account for these responses of SGC to AITC application, we applied AITC to neuron-free selective cultures of SGCs within 5 hr and 18 hr of dissociation from DRG. This showed similar

responses of SGCs isolated within 5 hr and 18 hr to those exposed to AITC in the presence of neurons (Figure 5n), indicating a direct action of AITC on SGCs.

We have previously observed that sensory neurons from rats and mice differ in their response to TRPA1 activation, with a higher percentage of responders among mouse neurons but greater amplitude of responses in rat neurons.<sup>67</sup> We therefore additionally measured AITC-induced  $[Ca^{2+}]_i$  rise in mouse DRG dissociated cultures. As previously reported,<sup>47</sup> the AITC-induced  $[Ca^{2+}]_i$  rise was absent in *TRPA1*<sup>-/-</sup> mice (Figure 6a to c), which confirms the specificity of AITC for TRPA1. A greater amplitude of  $[Ca^{2+}]_i$  response in rats compared to wild-type mice also duplicates prior findings.<sup>67</sup> We now show that this difference extends to SGCs, in which response to AITC stimulation in mouse SGCs is less than that observed in rat SGCs (Figure 6d to f). This likely reflects a species difference in TRPA1 channel expression and function between rat and mouse DRG cells.<sup>47,71,72</sup>

Taken together, our experimental results demonstrate that TRPA1 is functionally present in both DRG neurons and SGCs of rats and wild-type mice and that TRPA1 activation increases  $[Ca^{2+}]_i$  both by  $Ca^{2+}$  influx through the plasmalemma as well as by release of stored  $Ca^{2+}$ .

#### ***Painful peripheral inflammation and nerve injury increase TRPA1 membrane content in DRGs and elevate response to TRPA1 activation in neurons and SGCs***

We next asked whether painful conditions alter TRPA1 expression and function in sensory neurons and SGCs. We first analyzed and compared total TRPA1 protein levels in homogenates from DRG injected with saline or CFA. To evaluate the protein expression level of TRPA1 located in the DRG and intracellular trafficking alteration affected by the pain pathology, we separately examined TRPA1 protein levels in the NKA1 $\alpha$ -enriched membrane fraction versus the NKA1 $\alpha$ -deficient soluble fraction, hereafter referred to as PM and cytosolic fractions, respectively. These were extracted from the lumbar L4/L5 DRGs followed by semiquantitative immunoblotting of TRPA1 in these fractions. We additionally assessed whether CFA inflammatory pain and SNI-induced neuropathic pain modify intracellular responses to AITC in DRG neurons and SGCs of adult rats.

Inflammatory pain was induced in adult rats at six-week old age by intraplantar injection of CFA in the right hindpaw, which produced marked circumferential edema and redness of injected hindpaw,<sup>73</sup> reduced the threshold for withdrawal from mild (von Frey) and

noxious (Pin) mechanical stimuli, and increased sensitivity to heat, when compared with animals receiving only saline injection (Figure 7a to c). Signs of inflammation lasted throughout the 10-day testing duration. Immunoblot results from tissues collected 10 days after CFA injection showed that the total DRG homogenate TRPA1 was significantly increased compared to control (saline) (Figure 7d and e). Further analyses showed that TRPA1 was found in both PM and cytosolic fractions and that TRPA1 level in PM fractions from the DRG ipsilateral to CFA injection was significantly higher than in contralateral DRG (Figure 7f and g). We have also performed TRPA1 and GFAP colabeling on the ipsilateral L5 DRG sections from saline and CFA animals, and result showed an increased profile of TRPA1 expression in both neurons and GFAP-positive glial cells which are proliferated following CFA, compared to control (Figure S5). Functional assessment (application of AITC, 100  $\mu$ M) of the dissociated cultures from DRGs ipsilateral to CFA injection showed greater amplitude of  $[Ca^{2+}]_i$  responses to AITC in both DRG neurons (Figure 7h) and SGCs (both those attached to neurons and those alone, Figure 7i), compared to cells from saline injected DRG (Figure 7j).

Following nerve injury by SNI in rats operated on at six weeks of age, sensory testing revealed the expected pain behavior that included reduced threshold for withdrawal from von Frey testing representing mechanical allodynia, mechanical hyperalgesia during Pin testing, and increased sensitivity to heat stimulation (Figure 8a to c). These changes lasted throughout the four weeks testing interval. Immunoblot analysis of TRPA1 levels using DRG harvested four weeks after SNI revealed TRPA1 detection in both fractionized PM and cytosolic fractions. In the DRG ipsilateral to the nerve injury, the TRPA1 protein levels were significantly decreased in the cytosolic fractions but increased in the PM fractions, normalized to the corresponding fractions from contralateral L4/L5 DRG (Figure 8d and e). As with DRG proximal to CFA injection, both neurons and SGCs dissociated from DRG proximal to SNI showed increased  $Ca^{2+}$  response to TRPA1 stimulation, displaying increased  $[Ca^{2+}]_i$  and slower recovery evoked by AITC (100  $\mu$ M), compared to the control cells prepared from the sham-operated DRG (Figure 8f to h).

These data together indicate that inflammatory and neuropathic painful conditions trigger increased levels of TRPA1 in the PM levels and augmented TRPA1-induced  $Ca^{2+}$  signaling in both DRG neurons and SGCs.

## **Discussion**

Our experiments reveal several new findings. First, we show that TRPA1 expression in the peripheral nervous

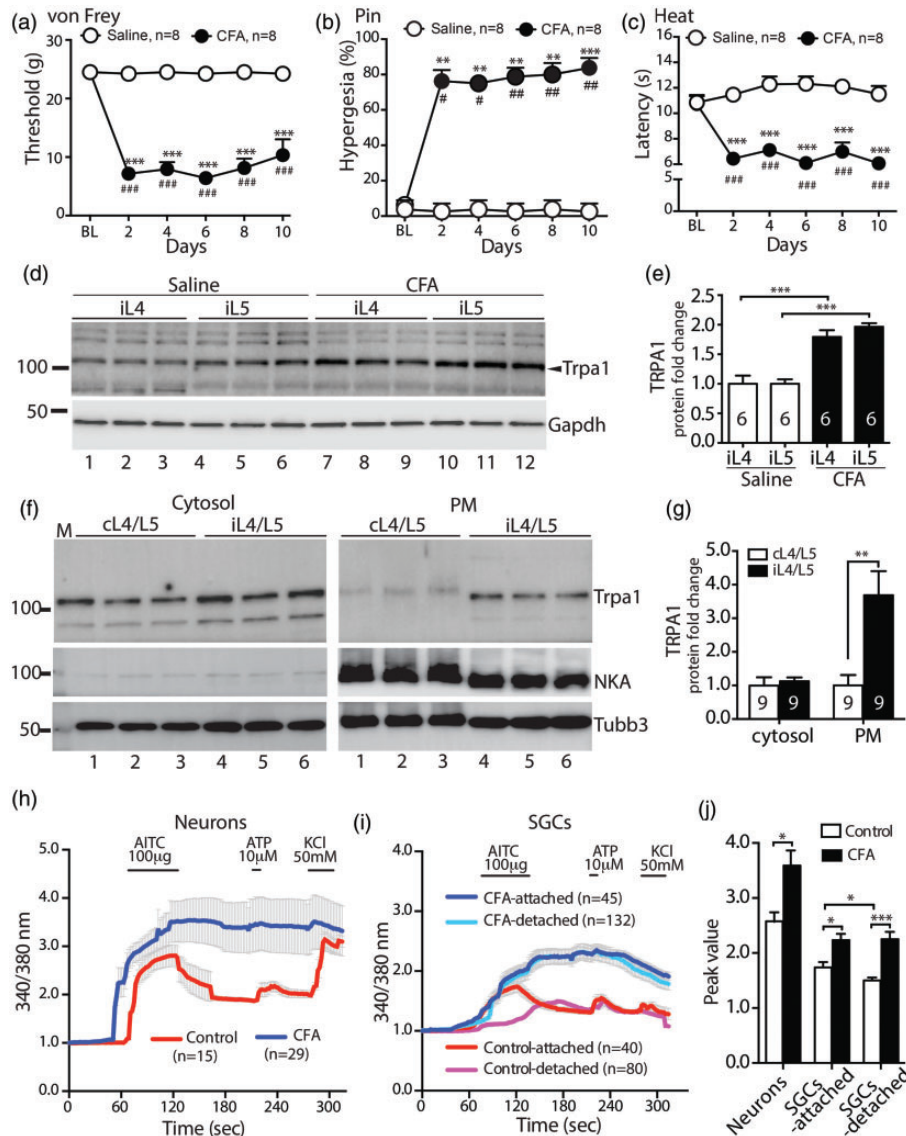


**Figure 7.** TRPA1 expression and activation in CFA-induced inflammatory pain. CFA rats developed mechanical allodynia (von Frey, a), hyperalgesia (Pin, b), and heat (c) hypersensitivity.  $^{\#}p < 0.05$ ,  $^{\#\#}p < 0.01$ , and  $^{\#\#\#}p < 0.001$  for comparison to baseline (BL) and  $^*p < 0.05$ ,  $^{**}p < 0.01$ , and  $^{***}p < 0.001$  for comparison between groups after CFA, respectively (repeated measures two-way ANOVA and Bonferroni post hoc tests for von Frey and heat, as well as nonparametric analyses by Friedman's test with Dunn's post hoc for Pin). Western blots show increased TRPA1 protein in L4 and L5 DRG homogenates of CFA, compared to saline (d), with bar charts (e) for densitometry analysis ( $^{***}p < 0.001$ , one-way ANOVA, Tuckey post hoc analysis). The number in each bar is the number of DRG per group). The NKA1 $\alpha$ -deficient cytosolic fraction and NKA1 $\alpha$ -enriched PM fraction were extracted from the DRG tissues at 10 days after CFA or vehicle injection and subjected to immunoblotting as shown in the representative immunoblots of TRPA1, NKA1 $\alpha$ , and Tubb3 of cytosol (f, left panels) and PM fractions (f, right panels), respectively. Bar charts (g) show densitometry analysis of immunoblots ( $^{***}p < 0.001$ , unpaired, two-tailed Student's *t*-test). The number in each bar is the number of analyzed DRGs per group. The  $[Ca^{2+}]_i$  response to AITC (100  $\mu$ M) in both neurons (h) and SGCs (i) from CFA rats ( $n=4$ ) was increased in magnitude and decay decreased compared to control cells. Bar chart (j) shows AITC-evoked peak values in neurons, as well as attached SGCs and detached SGCs ( $^*p < 0.05$  and  $^{***}p < 0.001$ , unpaired, two-tailed Student's *t*-test).

CFA: complete Freund's adjuvant; TRPA1: transient receptor potential cation channel subfamily A member 1; PM: plasma membrane; NKA: sodium/potassium ATPase; AITC: allyl isothiocyanate; SGC: satellite glial cell; GAPDH: glyceraldehyde 3-phosphate dehydrogenase.

system (PNS) is not restricted to primary sensory neurons in the DRG but is also expressed by the SGCs that surround the neuronal somata and SCs as reported.<sup>22,23</sup> In addition, we show that TRPA1 in SGCs is functional

and its activation increases SGC intracellular  $Ca^{2+}$ . Finally, we have found that TRPA1 expression and function in both SGCs and neurons are enhanced in models of inflammatory pain and neuropathic pain, as



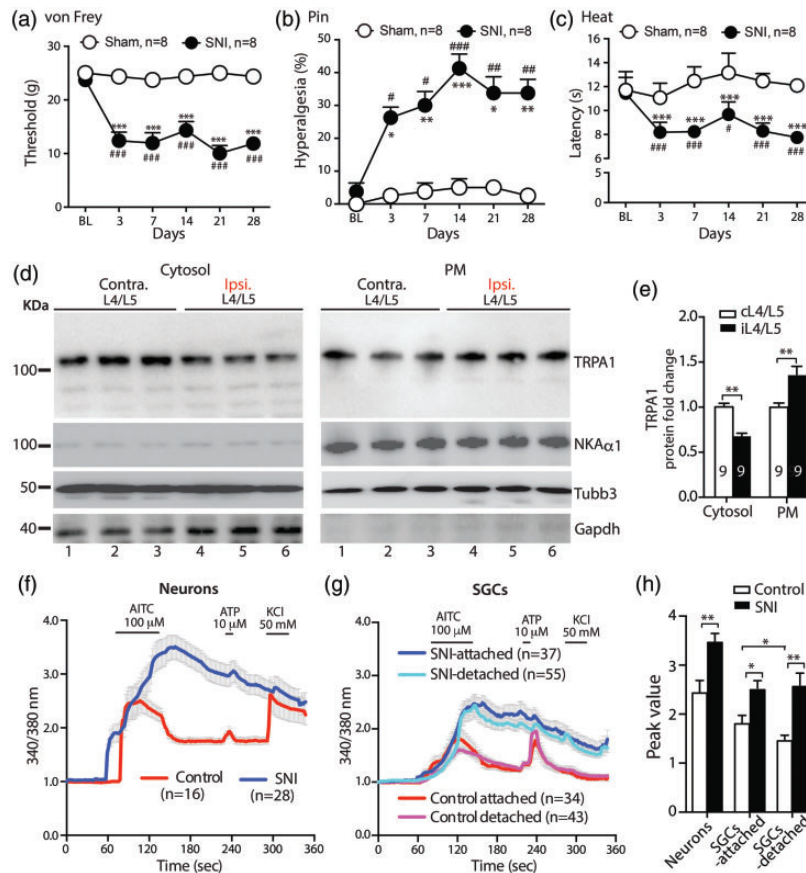


**Figure 8.** TRPA1 expression and activation in SNI-induced neuropathic pain. Rats with SNI developed mechanical allodynia (von Frey, a), hyperalgesia (Pin, b), and heat (c) hypersensitivity.  $^{\#}p < 0.05$ ,  $^{\#\#}p < 0.01$ , and  $^{\#\#\#}p < 0.001$  for comparison to baseline (BL) and  $^*p < 0.05$ ,  $^{**}p < 0.01$ , and  $^{***}p < 0.001$  for comparison between groups after SNI, respectively (repeated measures two-way ANOVA and Bonferroni post hoc tests for von Frey and heat, and nonparametric analyses by Friedman's test with Dunn's post hoc for Pin). The NKA1 $\alpha$ -eliminated cytosol and NKA1 $\alpha$ -enriched PM protein fractions were extracted from the DRG tissues at 28 days after SNI and control samples and subjected to immunoblotting as shown in the representative immunoblots of TRPA1, NKA1 $\alpha$ , and Tubb3 of cytosol (d, left panels) and PM fractions (d, right panels), respectively. Bar charts in the panel (e) are the results of densitometry analysis of immunoblots ( $^{**}p < 0.001$ , unpaired, two-tailed Student's *t*-test). The number in each bar is the number of analyzed DRG per group. In SNI L4/L5 DRG cultures ( $n=6$  animals), the  $[Ca^{2+}]_i$  after 1 min AITC (100  $\mu$ M) superfusion sequentially challenged with ATP (10  $\mu$ M) and KCl (50 mM), in SNI DRG culture, was markedly increased and  $[Ca^{2+}]_i$  decay decreased in both neurons (f) and SGCs (g), compared to the measurement in control DRG. Bar chart in the panel (h) is the results of averages of comparative quantification of AITC-evoked peak values in neurons and SGCs between SNI and controls in panels (f and g).  $^*p < 0.05$  and  $^{***}p < 0.001$  (unpaired, two-tailed Student's *t*-test).

SNI: spared nerve injury; TRPA1: transient receptor potential cation channel subfamily A member 1; PM: plasma membrane; NKA1 $\alpha$ : sodium/potassium ATPase 1 alpha; Tubb3:  $\beta$ 3-tubulin; GAPDH: glyceraldehyde 3-phosphate dehydrogenase; SGC: satellite glial cell; AITC: allyl isothiocyanate.

indicated by augmented AITC-evoked  $[Ca^{2+}]_i$  increases in the cell body and increased PM TRPA1 protein expression. These observations raise the possibility that TRPA1 in SGCs may contribute to the pathophysiology of both inflammatory and neuropathic pain.

Multiple published studies have shown TRPA1 cytoplasmic immunopositivity in the subpopulation of small-to medium-sized DRG neurons. However, as a multipass transmembrane protein that forms PM channels mediating  $Ca^{2+}$  influx, we would expect to find preferential localization of TRPA1 in the plasmalemma. Accordingly, using a well-validated extracellular loop-1

epitope TRPA1 antibody, we observe clear PM localization of TRPA1 in DRG neurons in both tissue sections and dissociated cultures. Several other reports also show that extracellular loop-1 epitope TRPA1 antibodies allow visualization of TRPA1 channels at the cell PM.<sup>38,56,74</sup> Moreover, we find that TRPA1 is also expressed by SGCs and nonmyelinating SCs. This is in accordance with recent reports that identified TRPA1 expression in SCs, where it contributes to the generation of neuropathic pain.<sup>22,23</sup> We also show function of these TRPA1 channels in SGCs dissociated from DRG by activation with the TRPA1-selective agonist AITC,

which produced influx of  $\text{Ca}^{2+}$  combined with release from intracellular stores. Furthermore, this response was abolished by the TRPA1-specific antagonist HC030031 and was absent in the SGCs and neurons from *Trpa1* null mice. Together, these data help support the findings that functional TRPA1 is expressed in SGCs.

SGCs and SCs are both derived from neural crest stem cells during embryonic development.<sup>6</sup> The former ensheath the primary sensory neurons, and the latter are divided into two types, either myelinating SCs that wrap large-diameter axons or nonmyelinating SCs that surround the nonmyelinated C fiber nociceptors. Both of these SC types support the maintenance and regeneration of axons of the neurons in the PNS.<sup>4,5</sup> Nonmyelinating S100-positive SCs are also a composition of perineuronal glial cells.<sup>6,15,75</sup> Furthermore, recent reports indicate that SGCs may represent a population of SC precursors.<sup>76–78</sup> Our observations that TRPA1 is also expressed by SGCs and nonmyelinating SCs further substantiate the relationship between these populations of nonneuronal cells in the DRG.

Previous reports have demonstrated a role for activation of TRPA1 receptors in chronic pain. It is known that inflammation and nerve injury increases TRPA1 expression in DRGs determined by immunoblots and quantitative PCR<sup>71,79–81</sup> and that augmented nociceptive signals can induce trafficking of neuronal TRPA1 to the PM.<sup>56,74,82,83</sup> We add further evidence showing that peripheral tissue inflammation and irreversible nerve injury can induce significant increases in the magnitude of the AITC-evoked  $[\text{Ca}^{2+}]_i$  transients in both SGCs as well as neurons. Although we are unable to quantitatively distinguish membrane TRPA1 levels separately in neurons and SGCs using the techniques employed in this study, it is known that TRPA1 translocation to the membrane represents a common mechanism controlling TRPA1 functionality in primary sensory neurons following inflammatory and peripheral nerve injury signals.<sup>56,74,82</sup> We speculate that inflammation and nerve injury induce SGC-TRPA1 sensitization that, together with neuron-TRPA1 activation, may contribute to pain by disrupting intracellular calcium signaling and ultimately cellular functions, which has been observed in models of neuropathic and inflammatory pain.<sup>46,80,84–86</sup> Recent studies have demonstrated communication between DRG neuronal somata and surrounding SGCs involving neuronal ATP release that induces SGC release of tumor necrosis factor alpha<sup>87</sup> and glutamate,<sup>88,89</sup> which in turn activate the neuronal population. It is therefore possible that SGC TRPA1 may be part of a similar signaling pathway that contributes to neuronal activation in pathological conditions.

In summary, our study demonstrates expression and function of TRPA1 in SGCs. Furthermore, our findings

indicate that peripheral inflammation and nerve injury induce SGC-TRPA1 activation that, together with elevated neuronal TRPA1 function, may contribute to increased primary afferent firing in persistent inflammatory or neuropathic pain. Genetic deletion of TRPA1 selectively from SCGs would allow dissection of the relative contribution of SGC-TRPA1 versus sensory neuron TRPA1.<sup>90</sup> Future studies could interrogate the cell-type specific TRPA1 roles within the DRG and trigeminal ganglia in models of soft tissue injury, nerve injury, or chronic disease.

### Author Contributions

Conceived and designed the experiments: HY and QHH. Performed the experiments: SMS, YC, CQ, BI-Z, BP, and HY. Analyzed the data: SMS, HY, and QHH. Funding acquisition: QHH, CLS, and HY. Wrote the paper: HY, CLS, and QHH.

### Declaration of Conflicting Interests

The author(s) declared no potential conflicts of interest with respect to the research, authorship, and/or publication of this article.

### Funding

The author(s) disclosed receipt of the following financial support for the research, authorship, and/or publication of this article: This research was supported by a grant from the Department of Veterans Affairs Rehabilitation Research and Development I01RX001940 (to QHH), a National Institutes of Health grants NS40538 (to CLS), and a Medical College of Wisconsin Neuroscience Research Center grant FP00016291 (to HY).

### ORCID iD

Hongwei Yu  <https://orcid.org/0000-0003-3029-3644>

### Supplemental Material

Supplemental material for this article is available online.

### References

1. Hogan QH. Labat lecture: the primary sensory neuron: where it is, what it does, and why it matters. *Reg Anesth Pain Med* 2010; 35: 306–311.
2. Guha D, Shamji MF. The dorsal root ganglion in the pathogenesis of chronic neuropathic pain. *Neurosurgery* 2016; 63(Suppl 1): 118–126.
3. Berta T, Qadri Y, Tan PH, Ji RR. Targeting dorsal root ganglia and primary sensory neurons for the treatment of chronic pain. *Expert Opin Ther Targets* 2017; 21: 695–703.
4. Pannese E. The structure of the perineuronal sheath of satellite glial cells (SGCs) in sensory ganglia. *Neuron Glia Biol* 2010; 6: 3–10.

5. Hanani, M. Satellite glial cells: more than just 'rings around the neuron'. *Neuron Glia Biol* 2010; 6: 1–2.
6. Hanani M. Satellite glial cells in sensory ganglia: from form to function. *Brain Res Brain Res Rev* 2005; 48: 457–476.
7. Hanani M. Intercellular communication in sensory ganglia by purinergic receptors and gap junctions: implications for chronic pain. *Brain Res* 2012; 1487: 183–191.
8. Poplawski G, Ishikawa T, Brifault C, Lee-Kubli C, Regestam R, Henry KW, Shiga Y, Kwon H, Ohtori S, Gonias SL, Campana WM. Schwann cells regulate sensory neuron gene expression before and after peripheral nerve injury. *Glia* 2018; 66: 1577–1590.
9. Milligan ED, Watkins LR. Pathological and protective roles of glia in chronic pain. *Nat Rev Neurosci* 2009; 10: 23–36.
10. Ji RR, Chamesian A, Zhang YQ. Pain regulation by non-neuronal cells and inflammation. *Science* 2016; 354: 572–577.
11. Ji RR, Xu ZZ, Gao YJ. Emerging targets in neuroinflammation-driven chronic pain. *Nat Rev Drug Discov* 2014; 13: 533–548.
12. Ferrari LF, Lotufo CM, Araldi D, Rodrigues MA, Macedo LP, Ferreira SH, Parada CA. Inflammatory sensitization of nociceptors depends on activation of NMDA receptors in DRG satellite cells. *Proc Natl Acad Sci USA* 2014; 111: 18363–18368.
13. Takeda M, Takahashi M, Matsumoto S. Contribution of the activation of satellite glia in sensory ganglia to pathological pain. *Neurosci Biobehav Rev* 2009; 33: 784–792.
14. Franke H, Verkhratsky A, Burnstock G, Illes P. Pathophysiology of astroglial purinergic signalling. *Purinergic Signal* 2012; 8: 629–657.
15. Wang F, Xiang H, Fischer G, Liu Z, Dupont MJ, Hogan QH, Yu H. HMG-CoA synthase isoenzymes 1 and 2 localize to satellite glial cells in dorsal root ganglia and are differentially regulated by peripheral nerve injury. *Brain Res* 2016; 1652: 62–70.
16. Rajasekhar P, Poole DP, Liedtke W, Bunnett NW, Veldhuis NA. P2Y1 receptor activation of the TRPV4 ion channel enhances purinergic signaling in satellite glial cells. *J Biol Chem* 2015; 290: 29051–29062.
17. Shigetomi E, Tong X, Kwan KY, Corey DP, Khakh BS. TRPA1 channels regulate astrocyte resting calcium and inhibitory synapse efficacy through GAT-3. *Nat Neurosci* 2011; 15: 70–80.
18. Shigetomi E, Jackson-Weaver O, Huckstepp RT, O'Dell TJ, Khakh BS. TRPA1 channels are regulators of astrocyte basal calcium levels and long-term potentiation via constitutive D-serine release. *J Neurosci* 2013; 33: 10143–10153.
19. Nassini R, Pedretti P, Moretto N, Fusi C, Carnini C, Facchinetti F, Viscomi AR, Pisano AR, Stokesberry S, Brunmark C, Svitacheva N, McGarvey L, Patacchini R, Damholt AB, Geppetti P, Materazzi S. Transient receptor potential ankyrin 1 channel localized to non-neuronal airway cells promotes non-neurogenic inflammation. *PLoS One* 2012; 7: e42454.
20. Gouin O, L'Herondelle K, Lebonvallet N, Le Gall-Ianotto C, Sakka M, Buhé V, Plée-Gautier E, Carré J-L, Lefeuve L, Misery L, Le Garrec R. TRPV1 and TRPA1 in cutaneous neurogenic and chronic inflammation: pro-inflammatory response induced by their activation and their sensitization. *Protein Cell* 2017; 8: 644–661.
21. Hamilton NB, Kolodziejczyk K, Kougioumtzidou E, Attwell D. Proton-gated Ca(2+)-permeable TRP channels damage myelin in conditions mimicking ischaemia. *Nature* 2016; 529: 523–527.
22. De Logu F, Li Puma S, Landini L, Portelli F, Innocenti A, de Araujo DSM, Janal MN, Patacchini R, Bunnett NW, Geppetti P, Nassini R. Schwann cells expressing nociceptive channel TRPA1 orchestrate ethanol-evoked neuropathic pain in mice. *J Clin Invest* 2019; 129: 5424–5441.
23. De Logu F, Nassini R, Materazzi S, Carvalho Gonçalves M, Nosi D, Rossi Degl'Innocenti D, Marone IM, Ferreira J, Li Puma S, Benemei S, Trevisan G, Souza Monteiro de Araújo D, Patacchini R, Bunnett NW, Geppetti P. Schwann cell TRPA1 mediates neuroinflammation that sustains macrophage-dependent neuropathic pain in mice. *Nat Commun* 2017; 8: 1887.
24. George D, Ahrens P, Lambert S. Satellite glial cells represent a population of developmentally arrested Schwann cells. *Glia* 2018; 66: 1496–1506.
25. Kerstein PC, del Camino D, Moran MM, Stucky CL. Pharmacological blockade of TRPA1 inhibits mechanical firing in nociceptors. *Mol Pain* 2009; 5: 19.
26. Kwan KY, Allchorne AJ, Vollrath MA, Christensen AP, Zhang D-S, Woolf CJ, Corey DP. TRPA1 contributes to cold, mechanical, and chemical nociception but is not essential for hair-cell transduction. *Neuron* 2006; 50: 277–289.
27. Gregory NS, Harris AL, Robinson CR, Dougherty PM, Fuchs PN, Sluka KA. An overview of animal models of pain: disease models and outcome measures. *J Pain* 2013; 14: 1255–1269.
28. Stein C, Millan MJ, Herz A. Unilateral inflammation of the hindpaw in rats as a model of prolonged noxious stimulation: alterations in behavior and nociceptive thresholds. *Pharmacol Biochem Behav* 1988; 31: 445–451.
29. Fischer G, Pan B, Vilceanu D, Hogan QH, Yu H. Sustained relief of neuropathic pain by AAV-targeted expression of CBD3 peptide in rat dorsal root ganglion. *Gene Ther* 2014; 21: 44–51.
30. Yu H, Fischer G, Jia G, Reiser J, Park F, Hogan QH. Lentiviral gene transfer into the dorsal root ganglion of adult rats. *Mol Pain* 2011; 7: 63.
31. Decosterd I, Woolf CJ. Spared nerve injury: an animal model of persistent peripheral neuropathic pain. *Pain* 2000; 87: 149–158.
32. Fischer G, Kostic S, Nakai H, Park F, Sapunar D, Yu H, Hogan Q. Direct injection into the dorsal root ganglion: technical, behavioral, and histological observations. *J Neurosci Methods* 2011; 199: 43–55.
33. Chaplan SR, Bach FW, Pogrel JW, Chung JM, Yaksh TL. Quantitative assessment of tactile allodynia in the rat paw. *J Neurosci Methods* 1994; 53: 55–63.
34. Wu HE, Gemes G, Zoga V, Kawano T, Hogan QH. Learned avoidance from noxious mechanical stimulation but not threshold Semmes Weinstein filament stimulation after nerve injury in rats. *J Pain* 2010; 11: 280–286.



35. Yu H, Fischer G, Ferhatovic L, Fan F, Light AR, Weihrauch D, Sapunar D, Nakai H, Park F, Hogan QH. Intraganglionic AAV6 results in efficient and long-term gene transfer to peripheral sensory nervous system in adult rats. *PLoS One* 2013; 8: e61266.
36. Gratzke C, Streng T, Waldkirch E, Sigl K, Stief C, Andersson K-E, Hedlund P. Transient receptor potential A1 (TRPA1) activity in the human urethra—evidence for a functional role for TRPA1 in the outflow region. *Eur Urol* 2009; 55: 696–704.
37. Earley S, Gonzales AL, Crnich R. Endothelium-dependent cerebral artery dilation mediated by TRPA1 and Ca<sup>2+</sup>-activated K<sup>+</sup> channels. *Circ Res* 2009; 104: 987–994.
38. Sullivan MN, Gonzales AL, Pires PW, Bruhl A, Leo MD, Li W, Oulidi A, Boop FA, Feng Y, Jaggar JH, Welsh DG, Earley S. Localized TRPA1 channel Ca<sup>2+</sup> signals stimulated by reactive oxygen species promote cerebral artery dilation. *Sci Signal* 2015; 8: ra2.
39. Meng Q, Fang P, Hu Z, Ling Y, Liu H. Mechanotransduction of trigeminal ganglion neurons innervating inner walls of rat anterior eye chambers. *Am J Physiol Cell Physiol* 2015; 309: C1–C10.
40. Yamamoto K, Chiba N, Chiba T, Kambe T, Abe K, Kawakami K, Utsunomiya I, Taguchi K. Transient receptor potential ankyrin 1 that is induced in dorsal root ganglion neurons contributes to acute cold hypersensitivity after oxaliplatin administration. *Mol Pain* 2015; 11: 69.
41. Xiang H, Liu Z, Wang F, Xu H, Roberts C, Fischer G, Stucky C, Caron D, Pan B, Hogan Q, Yu H. Primary sensory neuron-specific interference of TRPV1 signaling by AAV-encoded TRPV1 peptide aptamer attenuates neuropathic pain. *Mol Pain* 2017; 13: 1744806917717040.
42. Yu H, Pan B, Weyer A, Wu H-E, Meng J, Fischer G, Vilceanu D, Light AR, Stucky C, Rice F L, Hudmon A, Hogan Q. CaMKII controls whether touch is painful. *J Neurosci* 2015; 35: 14086–14102.
43. Li Q, Lau A, Morris TJ, Guo L, Fordyce CB, Stanley EF. A syntaxin 1, Galpha(o), and N-type calcium channel complex at a presynaptic nerve terminal: analysis by quantitative immunocolocalization. *J Neurosci* 2004; 24: 4070–4081.
44. Bhat NR, Shanker G, Pieringer RA. Investigations on myelination in vitro: regulation of 2,3'-cyclic nucleotide 3'-phosphohydrolase by thyroid hormone in cultures of dissociated brain cells from embryonic mice. *J Neurochem* 1981; 37: 695–701.
45. Hammond DL, Ackerman L, Holdsworth R, Elzey B. Effects of spinal nerve ligation on immunohistochemically identified neurons in the L4 and L5 dorsal root ganglia of the rat. *J Comp Neurol* 2004; 475: 575–589.
46. Gemes G, Bangaru MLY, Wu H-E, Tang Q, Weihrauch D, Koopmeiners AS, Cruikshank JM, Kwok W-M, Hogan QH. Store-operated Ca<sup>2+</sup> entry in sensory neurons: functional role and the effect of painful nerve injury. *J Neurosci* 2011; 31: 3536–3549.
47. Barabas ME, Kossyeva EA, Stucky CL. TRPA1 is functionally expressed primarily by IB4-binding, non-peptidergic mouse and rat sensory neurons. *PLoS One* 2012; 7: e47988.
48. Marsakova L, Barvik I, Zima V, Zimova L, Vlachova V. The first extracellular linker is important for several aspects of the gating mechanism of human TRPA1 channel. *Front Mol Neurosci* 2017; 10: 16.
49. Duncan C, Mueller S, Simon E, Renger JJ, Uebele VN, Hogan QH, Wu H-E. Painful nerve injury decreases sarcoplasmic reticulum Ca(2+)-ATPase activity in axotomized sensory neurons. *Neuroscience* 2013; 231: 247–257.
50. Sonnemann KJ, Heun-Johnson H, Turner AJ, Baltgalvis KA, Lowe DA, Ervasti JM. Functional substitution by TAT-utrophin in dystrophin-deficient mice. *PLoS Med* 2009; 6: e1000083.
51. Liu Z, Wang F, Fischer G, Hogan QH, Yu H. Peripheral nerve injury induces loss of nociceptive neuron-specific Galphai-interacting protein in neuropathic pain rat. *Mol Pain* 2016; 4: 12.
52. Xiang H, Xu H, Fan F, Shin SM, Hogan QH, Yu H. Glial fibrillary acidic protein promoter determines transgene expression in satellite glial cells following intraganglionic adeno-associated virus delivery in adult rats. *J Neurosci Res* 2018; 96: 436–448.
53. Wang S, Kobayashi K, Kogure Y, Yamanaka H, Yamamoto S, Yagi H, Noguchi K, Dai Y. Negative regulation of TRPA1 by AMPK in primary sensory neurons as a potential mechanism of painful diabetic neuropathy. *Diabetes* 2018; 67: 98–109.
54. Derouiche S, Mariot P, Warnier M, Vancauwenberghe E, Bidaux G, Gosset P, Mauroy B, Bonnal J-L, Slomianny C, Delcourt P, Dewailly E, Prevarskaya N, Roudbaraki M. Activation of TRPA1 channel by antibacterial agent triclosan induces VEGF secretion in human prostate cancer stromal cells. *Cancer Prev Res (Phila)* 2017; 10: 177–187.
55. Berrout J, Kyriakopoulou E, Moparthi L, Hoge A, Berrout L, Ivan C, Lorgier M, Boyle J, Peers C, Muench S, Gomez JE, Hu X, Hurst C, Hall T, Umamaheswaran S, Wesley L, Gagea M, Shires M, Manfield I, Knowles MA, Davies S, Suhling K, Gonzalez YT, Carragher N, Macleod K, Abbott NJ, Calin GA, Gamper N, Zygmunt PM, Timsah Z. TRPA1-FGFR2 binding event is a regulatory oncogenic driver modulated by miRNA-142-3p. *Nat Commun* 2017; 8: 947.
56. Meng J, Wang J, Steinhoff M, Dolly JO. TNFalpha induces co-trafficking of TRPV1/TRPA1 in VAMP1-containing vesicles to the plasmalemma via Munc18-1/syntaxin1/SNAP-25 mediated fusion. *Sci Rep* 2016; 6: 21226.
57. Xu Y, Jia J, Xie C, Wu Y, Tu W. Transient receptor potential ankyrin 1 and substance P mediate the development of gastric mucosal lesions in a water immersion restraint stress rat model. *Digestion* 2018; 97: 228–239.
58. Steiner C, Gevaert T, Ganzer R, De Ridder D, Neuhaus J. Comparative immunohistochemical characterization of interstitial cells in the urinary bladder of human, guinea pig and pig. *Histochem Cell Biol* 2018; 149: 491–501.
59. Uckert S, Sonnenberg JE, Albrecht K, Kuczyk MA, Hedlund P. Expression and distribution of the transient receptor potential cationic channel ankyrin 1 (TRPA1) in the human vagina. *Int J Impot Res* 2015; 27: 16–19.

60. Chukyo A, Chiba T, Kambe T, Yamamoto K, Kawakami K, Taguchi K, Abe K. Oxaliplatin-induced changes in expression of transient receptor potential channels in the dorsal root ganglion as a neuropathic mechanism for cold hypersensitivity. *Neuropeptides* 2018; 67: 95–101.
61. Marics B, Peitl B, Varga A, Pázmándi K, Bácsi A, Németh J, Szilvássy Z, Jancsó G, Dux M. Diet-induced obesity alters dural CGRP release and potentiates TRPA1-mediated trigeminovascular responses. *Cephalalgia* 2017; 37: 581–591.
62. Haas ET, Rowland K, Gautam M. Tooth injury increases expression of the cold sensitive TRP channel TRPA1 in trigeminal neurons. *Arch Oral Biol* 2011; 56: 1604–1609.
63. Weinhold P, Gratzke C, Streng T, Stief C, Andersson KE, Hedlund P. TRPA1 receptor induced relaxation of the human urethra involves TRPV1 and cannabinoid receptor mediated signals, and cyclooxygenase activation. *J Urol* 2010; 183: 2070–2076.
64. Pannese E. The structure of the perineuronal sheath of satellite glial cells (SGCs) in sensory ganglia. *Neuron Glia Biol* 2010; 6: 3–10.
65. Campana WM. Schwann cells: activated peripheral glia and their role in neuropathic pain. *Brain Behav Immun* 2007; 21: 522–527.
66. Kwan KY, Glazer JM, Corey DP, Rice FL, Stucky CL. TRPA1 modulates mechanotransduction in cutaneous sensory neurons. *J Neurosci* 2009; 29: 4808–4819.
67. Barabas ME, Stucky CL. TRPV1, but not TRPA1, in primary sensory neurons contributes to cutaneous incision-mediated hypersensitivity. *Mol Pain* 2013; 9: 9.
68. Suadicani SO, Cherkas PS, Zuckerman J, Smith DN, Spray DC, Hanani M. Bidirectional calcium signaling between satellite glial cells and neurons in cultured mouse trigeminal ganglia. *Neuron Glia Biol* 2010; 6: 43–51.
69. Verderio C, Matteoli M. ATP in neuron-glia bidirectional signalling. *Brain Res Rev* 2011; 66: 106–114.
70. Shang S, Zhu F, Liu B, Chai Z, Wu Q, Hu M, Wang Y, Huang R, Zhang X, Wu X, Sun L, Wang Y, Wang L, Xu H, Teng S, Liu B, Zheng L, Zhang C, Zhang F, Feng X, Zhu D, Wang C, Liu T, Zhu MX, Zhou Z. Intracellular TRPA1 mediates Ca<sup>2+</sup> release from lysosomes in dorsal root ganglion neurons. *J Cell Biol* 2016; 215: 369–381.
71. Obata K, Katsura H, Mizushima T, Yamanaka H, Kobayashi K, Dai Y, Fukuoka T, Tokunaga A, Tominaga M, Noguchi K. TRPA1 induced in sensory neurons contributes to cold hyperalgesia after inflammation and nerve injury. *J Clin Invest* 2005; 115: 2393–2401.
72. Chen J, Kang D, Xu J, Lake M, Hogan JO, Sun C, Walter K, Yao B, Kim D. Species differences and molecular determinant of TRPA1 cold sensitivity. *Nat Commun* 2013; 4: 2501.
73. Fehrenbacher JC, Vasko MR, Duarte DB. Models of inflammation: carrageenan- or complete Freund's adjuvant (CFA)-induced edema and hypersensitivity in the rat. *Curr Protoc Pharmacol* 2012; 56.
74. Schmidt M, Dubin AE, Petrus MJ, Earley TJ, Patapoutian A. Nociceptive signals induce trafficking of TRPA1 to the plasma membrane. *Neuron* 2009; 64: 498–509.
75. Armati PJ, Mathey EK. An update on Schwann cell biology—immunomodulation, neural regulation and other surprises. *J Neurol Sci* 2013; 333: 68–72.
76. George D, Ahrens P, Lambert S. Satellite glial cells represent a population of developmentally arrested Schwann cells. *Glia* 2018; 66: 1496–1506.
77. Uesaka T, Nagashimada M, Enomoto H. Neuronal differentiation in Schwann cell lineage underlies postnatal neurogenesis in the enteric nervous system. *J Neurosci* 2015; 35: 9879–9888.
78. Fex Svenningsen A, Colman DR, Pedraza L. Satellite cells of dorsal root ganglia are multipotential glial precursors. *Neuron Glia Biol* 2004; 1: 85–93.
79. da Costa DS, Meotti FC, Andrade EL, Leal PC, Motta EM, Calixto JB. The involvement of the transient receptor potential A1 (TRPA1) in the maintenance of mechanical and cold hyperalgesia in persistent inflammation. *Pain* 2010; 148: 431–437.
80. Lu SG, Gold MS. Inflammation-induced increase in evoked calcium transients in subpopulations of rat dorsal root ganglion neurons. *Neuroscience* 2008; 153: 279–288.
81. Lennertz RC, Kossyeva EA, Smith AK, Stucky CL. TRPA1 mediates mechanical sensitization in nociceptors during inflammation. *PLoS One* 2012; 7: e43597.
82. Vilceanu D, Stucky CL. TRPA1 mediates mechanical currents in the plasma membrane of mouse sensory neurons. *PLoS One* 2010; 5: e12177.
83. Bautista DM, Jordt S-E, Nikai T, Tsuruda PR, Read AJ, Poblete J, Yamoah EN, Basbaum AI, Julius D. TRPA1 mediates the inflammatory actions of environmental irritants and proalgesic agents. *Cell* 2006; 124: 1269–1282.
84. Bagur R, Hajnoczky G. Intracellular Ca(2+) sensing: its role in calcium homeostasis and signaling. *Mol Cell* 2017; 66: 780–788.
85. Faber ES, Sah P. Calcium-activated potassium channels: multiple contributions to neuronal function. *Neuroscientist* 2003; 9: 181–194.
86. Miller RJ. Multiple calcium channels and neuronal function. *Science* 1987; 235: 46–52.
87. Zhang X, Chen Y, Wang C, Huang LY. Neuronal somatic ATP release triggers neuron-satellite glial cell communication in dorsal root ganglia. *Proc Natl Acad Sci USA* 2007; 104: 9864–9869.
88. Rozanski GM, Li Q, Stanley EF. Transglial transmission at the dorsal root ganglion sandwich synapse: glial cell to postsynaptic neuron communication. *Eur J Neurosci* 2013; 37: 1221–1228.
89. Rozanski GM, Li Q, Kim H, Stanley EF. Purinergic transmission and transglial signaling between neuron somata in the dorsal root ganglion. *Eur J Neurosci* 2013; 37: 359–365.
90. Zappia KJ, O'Hara CL, Moehring F, Kwan KY, Stucky CL. Sensory neuron-specific deletion of TRPA1 results in mechanical cutaneous sensory deficits. *eNeuro* 2017; 4: pii: ENEURO.0069-16.2017.